Received: 20 September 2023 | Revised: 30 January 2024 | Accepted: 3 February 2024

DOI: 10.1002/cac2.12523

CANCER COMMUNICATIONS Open Access

ORIGINAL ARTICLE

NAT10-mediated ac^{4}C-modified ANKZF1 promotes tumor progression and lymphangiogenesis in clear-cell renal cell carcinoma by attenuating YWHAE-driven cytoplasmic retention of YAP1

Daojia Miao[1,2] | **Jian Shi**[1,2] | **Qingyang Lv**[1,2] | **Diaoyi Tan**[1,2] | **Chuanyi Zhao**[1,2] | **Zhiyong Xiong**[1,2] | **Xiaoping Zhang**[1,2]

[1]Department of Urology, Union Hospital, Tongji Medical College, Huazhong University of Science and Technology, Wuhan, Hubei, P. R. China

[2]Institute of Urology, Union Hospital, Tongji Medical College, Huazhong University of Science and Technology, Wuhan, Hubei, P. R. China

Correspondence
Xiaoping Zhang and Zhiyong Xiong, Department of Urology, Union Hospital, Tongji Medical College, Huazhong University of Science and Technology, Wuhan 430022, Hubei, P. R. China.
Email: xzhang@hust.edu.cn and tjxiongzhiyong@163.com

Funding information
National Natural Science Foundation of China, Grant/Award Numbers: 81874090, 81972630, 82202911, 82300786

Abstract

Background: Lymphatic metastasis is one of the most common metastatic routes and indicates a poor prognosis in clear-cell renal cell carcinoma (ccRCC). N-acetyltransferase 10 (NAT10) is known to catalyze N4-acetylcytidine (ac^{4}C) modification of mRNA and participate in many cellular processes. However, its role in the lymphangiogenic process of ccRCC has not been reported. This study aimed to elucidate the role of NAT10 in ccRCC lymphangiogenesis, providing valuable insights into potential therapeutic targets for intervention.

Methods: ac^{4}C modification and NAT10 expression levels in ccRCC were assessed using public databases and clinical samples. Functional investigations involved manipulating NAT10 expression in cellular and mouse models to study its role in ccRCC. Mechanistic insights were gained through a combination of RNA sequencing, mass spectrometry, co-immunoprecipitation, RNA immunoprecipitation, immunofluorescence, and site-specific mutation analyses.

Results: We found that ac^{4}C modification and NAT10 expression levels increased in ccRCC. NAT10 promoted tumor progression and lymphangiogenesis of ccRCC by enhancing the nuclear import of Yes1-associated transcriptional regulator (YAP1). Subsequently, we identified ankyrin repeat and zinc fin-

List of abbreviations: ANKZF1, ankyrin repeat and zinc finger peptidyl tRNA hydrolase 1; ac^{4}C, N4-acetylcytidine; ccRCC, clear-cell renal cell carcinoma; cDNA, complementary DNA; co-IP, co-immunoprecipitation; CPTAC-3, clinical proteomic tumor analysis consortium 3; DAPI, 4',6-diamidino-2-phenylindole; FDR, false discovery rate; *GAPDH*, glyceraldehyde-3-phosphate dehydrogenase; GSEA, gene set enrichment analysis; HLEC, human lymphatic endothelial cell; HR, hazard ratio; ICGC-RECA, international cancer genome consortium-renal clear-cell carcinoma; IHC, immunohistochemical; KEGG, Kyoto encyclopedia of genes and genomes; KIRC, kidney renal clear-cell carcinoma; LATS1/2, large tumor suppressor kinase 1/2; LYVE1, lymphatic vessel endothelial hyaluronan receptor 1; MS, mass spectrometry; NAT10, N-acetyltransferase 10; NES, normalized enrichment score; NF2, moesin-ezrin-radixin like tumor suppressor; PE, phycoerythrin; TCGA, the cancer genome atlas; VEGFC/D, vascular endothelial growth factor C/D; YAP1, Yes1-associated transcriptional regulator; YWHAE, tyrosine 3-monooxygenase/tryptophan 5-monooxygenase activation protein epsilon; TAZ, tafazzin; 7-AAD, 7-amino-actinomycin D.

Daojia Miao, Jian Shi, Qingyang Lv, and Diaoyi Tan contributed equally to this study.

ger peptidyl tRNA hydrolase 1 (ANKZF1) as the functional target of NAT10, and its upregulation in ccRCC was caused by NAT10-mediated ac^{4}C modification. Mechanistic analyses demonstrated that ANKZF1 interacted with tyrosine 3-monooxygenase/tryptophan 5-monooxygenase activation protein epsilon (YWHAE) to competitively inhibit cytoplasmic retention of YAP1, leading to transcriptional activation of pro-lymphangiogenic factors.

Conclusions: These results suggested a pro-cancer role of NAT10-mediated acetylation in ccRCC and identified the NAT10/ANKZF1/YAP1 axis as an under-reported pathway involving tumor progression and lymphangiogenesis in ccRCC.

KEYWORDS

clear-cell renal cell carcinoma, N4-acetylcytidine, N-acetyltransferase 10, YAP1 nuclear import

1 | BACKGROUND

More than 430,000 new cases of kidney cancer were diagnosed in 2020 worldwide [1]. Clear-cell renal cell carcinoma (ccRCC) accounts for more than 70% of all kidney cancers [2]. As the most frequent histological type of kidney cancer, ccRCC has long been characterized by its high mortality, leading to an estimated 13,000 related deaths in 2020 in the USA [3]. Currently, for localized ccRCC, surgical excision is the only curative treatment because of its remarkable clinical outcomes [4]. However, approximately a third of ccRCC patients at their first hospital diagnosis will present with metastases which cause a low 5-year survival rate [5, 6]. It is noteworthy that among all patients with metastatic ccRCC, approximately half (45%) of them exhibit lymph node involvement [7]. Thus, it is urgently needed to investigate the mechanisms of ccRCC development and metastasis, as well as to discover new therapeutic targets.

Lymphangiogenesis is a highly complicated process in which newborn lymphatic vessels sprout from the existing ones and holds significant importance in various pathological contexts, including cancer [8–10]. Initially, it was thought that lymphatic vessels were almost absent within tumors [11]. Even though it was later discovered that lymphatic vessels do exist within tumors, they were regarded as a drainage system for the tumor interstitial fluid [12]. Currently, an increasing body of evidence suggests that tumor-induced lymphangiogenesis stimulates the growth of lymphatic vessels both within and surrounding the tumor, thereby facilitating the spread of tumor cells to adjacent regional lymph nodes in various cancer models [9, 13, 14]. Comparable to tumor-induced angiogenesis, lymphangiogenesis is an active biological behavior of tumors and is governed by pro-lymphangiogenic factors secreted by cancer cells [15]. Among all known pro-lymphangiogenic factors, vascular endothelial growth factor-C/D (VEGFC/D) plays the most important role in tumor lymphangiogenesis [16]. As a receptor tyrosine kinases expressed on the surface of lymphatic endothelial cells, VEGFR3, when activated by VEGFC/D, induces the proliferation of lymphatic endothelial cells in vitro and lymphangiogenesis in vivo [17]. In addition, autocrine signaling by VEGFC/D-VEGFR3 promotes tumor growth and invasion through multiple mechanisms, such as activation of oncogenes, modulation of the inflammatory tumor microenvironment, and promotion of immune escape [18]. Although several groups have reported that tumor lymphangiogenesis was closely associated with lymph node metastasis and patients' survival in renal cancer [19–21], few comprehensive studies on its regulatory mechanisms have been conducted. Thus, it necessitates investigating the potential regulator involved in tumor lymphangiogenesis by preventing lymphatic metastasis and providing a more efficient therapeutic strategy for ccRCC.

N-acetyltransferase 10 (NAT10), first reported in 2003 by Lv et al. [22], is a member of the Gcn5-related N-acetyltransferase family. As a lysine acetyltransferase, NAT10 catalyzes N4-acetylcytidine (ac^{4}C) modification at the cytidine site on RNA [23]. ac^{4}C, an evolutionarily conserved chemical modification of RNA, was first described in yeast [24] and *Escherichia coli* [25]. As with numerous RNA modifications, ac^{4}C was discovered initially in transfer RNA and ribosomal RNA, and subsequently identified in mRNA [26]. Recently, ac^{4}C has been considered a prevalently epigenetic marker of mRNAs, which can influence mRNA stabilities and translation efficiencies [26, 27]. Newly emerging studies have coupled NAT10-mediated deposition of ac^{4}C to cancer development [28, 29], and it is suggested that NAT10 promoted

tumor progression by regulating ferroptosis in colon cancer [29]. Additionally, previous studies have proposed that NAT10-medicated ac^4C modification enhanced tumorigenic activities by upregulating the mutant *p53* level or inhibiting cell cycle arrest [28, 30]. Although a previous study claimed that NAT10 was upregulated in ccRCC [31], the role of both NAT10 and ac^4C modification in ccRCC remains largely unknown. Particularly, their relationship with tumor lymphangiogenesis has not been reported.

Here, we evaluated the NAT10 expression and NAT10-mediated ac^4C modification levels in ccRCC. Subsequently, the roles of NAT10 in ccRCC progression and lymphangiogenesis were explored by in vitro and in vivo assays. Finally, we carefully investigated the mechanism underlying NAT10-regulated ccRCC development and lymphangiogenesis.

2 | METHODS AND MATERIALS

2.1 | Patient samples and human cell lines

Tumors and adjacent normal tissues were obtained from 36 patients diagnosed with ccRCC at Union Hospital (Wuhan, Hubei, China) between July 2020 and July 2022. None of these patients underwent radiotherapy or chemotherapy before the nephrectomy. Written informed consent was obtained from all patients, and the present study was authorized by the ethics committee of Union Hospital (IEC-072).

Human embryonic kidney 293T (HEK293T) cells, renal proximal tubule epithelial cells (RPTEC), ccRCC cells (A498, 786-O, CAKI-1, and OSRC-2), and lymphatic endothelial cells (HLECs) were purchased from the American Type Culture Collection (Manassas, VA, USA). These cell lines were confirmed by short tandem repeat profiling in August 2021. HEK293T, RPTEC, and ccRCC cells were cultured in Dulbecco's modified eagle medium (DMEM, Gibco, Waltham, MA, USA) supplemented with 10% fetal bovine serum (FBS, Gibco) at 37°C under 5% CO_2. HLECs were cultured in the endothelial cell medium with 5% FBS. Moreover, the conditioned medium (CM) from ccRCC cells was centrifuged at 200 ×g for 5 min and applied to culture HLECs.

2.2 | Real-time PCR

Total RNA was isolated from ccRCC tissues and cell lines with Trizol solution (#R0016, Beyotime, Shanghai, China). The cDNA was synthesized with a First Strand Synthesis Kit (#R212-02, Vazyme, Nanjing, Jiangsu, China), and qPCR was performed with a Sybr Green Kit (#RK21203, ABclonal, Wuhan, Hubei, China) on qTOWER Thermocycler (Analytik Jena, Jena, Germany) following the conditions: 95°C for 3 min, 45 cycles of 95°C for 5 s and 60°C for 30 s. Relative mRNA levels were calculated using the $2^{-\Delta\Delta Ct}$ method. Primers were synthesized by Tsingke (Beijing, China), and their sequences are listed in Supplementary Table S1.

2.3 | Western blotting and co-immunoprecipitation (co-IP)

A total of 30 μg protein extracted from ccRCC tissues and cell lines was loaded on polyacrylamide gels. Then, these proteins were transferred onto polyvinylidene fluoride membranes (Roche, Basel, Switzerland). After incubating with primary antibodies at 4°C for 12-14 h, the membranes were incubated with corresponding secondary antibodies for 2 h. These membranes were visualized by a ChemiDoc imaging system (Bio-Rad, Hercules, CA, USA).

For co-IP assays, ccRCC cells were lysed and incubated with IgG or primary antibodies overnight at 4°C. Then protein A/G magnetic beads (#HY-K0202, MedChemExpress, Monmouth Junction, NJ, USA) were added to the mixtures of cell lysates and antibodies. After incubating for 2 h at room temperature, the mixtures were washed to remove non-specifically bound immune complexes. Finally, the remaining immune complexes were separated by Western blotting. The list of antibodies is provided in Supplementary Table S2.

2.4 | Transfection and infection

The small interfering RNA (siRNA) was purchased from GenePharma (Shanghai, China). NAT10-overexpressed and ankyrin repeat and zinc finger peptidyl tRNA hydrolase 1 (ANKZF1)-overexpressed lentiviruses and short hairpin RNA (shRNA) were purchased from GeneChem (Shanghai, China). The human Myc-tyrosine 3-monooxygenase/tryptophan 5-monooxygenase activation protein epsilon (Myc-YWHAE) plasmid and truncated plasmids of Flag-ANKZF1 were synthesized by GeneChem. Transfections were performed using Lipofectamine 6000 (#C0526, Beyotime), and infections were conducted using the Hitrans AP reagent (GeneChem) with the guidance of the manufacturer's protocol. Additionally, dual siRNAs or shRNAs were uniquely designed for each target, as delineated in Supplementary Table S3. The knockdown efficiency of each siRNA or shRNA was assessed through qPCR, and the one demonstrating the

higher gene knockdown efficiency was selectively utilized in subsequent assays.

2.5 | Animal models

BALB/c nude mice (male, 5-week-old) were purchased from Hua Fukang (Beijing, China) and maintained under a specific pathogen-free barrier environment. The animal study was approved by the Animal Care and Use Committee of Union Hospital (S3694).

The subcutaneous tumor model was created by subcutaneously injecting 2×10^6 CAKI-1 cells into nude mice ($n = 5$). At 44 days post-injection or upon reaching a subcutaneous tumor diameter exceeding 1.5 cm, humane euthanasia was performed using CO_2 followed by cervical dislocation. Then the subcutaneous tumors were photographed and weighed.

The metastatic tumor model was established by injecting 4×10^6 A498 cells into the tail veins of nude mice ($n = 5$). After 8 weeks, the LagoX system (Spectral Instruments Imaging, Tucson, AZ, USA) was applied to visualize the nude mice.

2.6 | Tube formation assays

HLECs (8×10^4) suspended in CM from ccRCC cells were seeded into a Matrigel-coated 48-well plate. After 8 h culture, HLECs were washed with phosphate-buffered saline (PBS) and stained with Calcein-AM (#HY-D0041, MedChemExpress). Then the tube-like structure on the growth factor-reduced Matrigel was photographed by a microscope (#DMI3000B, Leica, Wetzlar, Hessen, Germany). The total tube length and the number of junctions were analyzed using the ImageJ software (National Institutes of Health, Bethesda, MD, USA).

2.7 | Enzyme-linked immunosorbent assay (ELISA)

The VEGFC/D concentrations in CM from ccRCC cells were detected using human VEGFC/D ELISA Kits (#E-EL-H1600c and #E-EL-H1601c, Elabscience, Wuhan, Hubei, China) following the manufacturer's protocol. Briefly, diluent CM (dilution ratio = 5) was pipetted to a 96-well plate pre-coated with the capture antibody. The absorbance at 450 nm was measured by a spectrophotometer (NanoDrop Technologies, Wilmington, DE, USA) and used to calculate the VEGFC/D concentrations.

2.8 | Dot blotting

In brief, a total of 50 ng mRNA from tumor tissues and ccRCC cells was spotted on the Nitrocellulose membrane (Biosharp, Hefei, Anhui, China) after mRNA purification. Then, the membranes were cross-linked in an oven at 60°C for 2 h and incubated with the ac^4C antibody at 4°C overnight. The corresponding secondary antibodies were subsequently added to the nitrocellulose membrane at room temperature for 2 h. Finally, the membrane was visualized by the ChemiDoc imaging system.

2.9 | RNA immunoprecipitation (RIP) and RNA-sequencing (RNA-seq)

NAT10-RIP and ac^4C-RIP assays were performed according to the protocols of the Magna RIP Kit (#17-700, Millipore, Burlington, MA, USA). Extracted from the products of RIP assays and ccRCC cells, RNA samples were prepared for RNA-seq analysis. RNA-seq analysis were provided by Bioyi Biotechnology Co., Ltd. (Wuhan, Hubei, China). The list of antibodies is provided in Supplementary Table S2.

2.10 | ac^4C-RIP-qPCR

Total RNA extraction from ccRCC tissues and cell lines was performed using the Trizol solution. Following this, polyadenylated RNA was enriched from the total RNA using mRNA capture beads included in the mRNA library prep kit (#12301ES24, Yeasen, Shanghai, China). Random RNA fragmentation was carried out using the RNA fragmentation reagents also provided in the mRNA library prep kit. In brief, 4 μg of mRNA was equally distributed between the input and ac^4C-RIP groups. For the ac^4C-RIP group, 2 μg of mRNA underwent incubation with the ac^4C antibody and was diluted into 500 μL ac^4C-RIP buffer. Following that, protein A/G magnetic beads were introduced to the mixture, undergoing rotation at room temperature for 2 h. After four rinses with ac^4C-RIP buffer, the ac^4C-RIP fraction was utilized to isolate ac^4C-RIP mRNA through Trizol and ethanol precipitation. Finally, RT-qPCR was performed using PCRMix (#R323-01, #Q341, Vazyme) for ac^4C-RIP mRNA and Input mRNA. The thermal cycling profile consisted of an initial denaturation at 95°C for 3 min, followed by 45 cycles of 95°C for 5 s and 60°C for 30 s. The relative mRNA level was determined based on the number of amplification cycles (Cq). The calculation formula is as follows:

$$\Delta Cq_{(Control)} = Cq_{(ac^4C-RIP)} - Cq_{(Input)}; \Delta Cq_{(Treatment)} = Cq_{(ac^4C-RIP)} - Cq_{(Input)}$$

$$Relative ac^4C modification level = 2^{\Delta CT(Control)-\Delta CT(Treatment)}.$$

2.11 | mRNA stability assays

ccRCC cells were plated in 6-well plates (50% confluency) and incubated for 24 h. Post-treatment with 5 μg/mL actinomycin D (#HY-17559, MedChemExpress) for 0, 2, 4, 6, 8, or 10 h, cells were harvested for RNA extraction. Subsequently, RT-qPCR was performed to calculate mRNA half-life, determined by the Cq value.

2.12 | Cell viability assays

ccRCC cells and HLECs were seeded in a 96-well plate (2,000 cells/well). To assess cell proliferation, Cell Counting Kits (CCK8, #40203ES76, Yeasen) were employed. A mixture of 10 μL of CCK8 solution and 100 μL of DMEM was added to each well, followed by incubation in darkness at 37°C. The absorbance at 450 nm was recorded at 0, 24, 48, 72, and 96 h using the NanoDrop spectrophotometer.

2.13 | Colony formation assays

In brief, ccRCC cells were seeded in 6-well plates (1,000 cells/well). After a 2-week incubation, cells underwent PBS rinsing, methanol fixation, and staining with 0.05% crystal violet (#G1014, Servicebio, Wuhan, Hubei, China). Finally, colonies were photographed on day 14. The colony formation rate (%) = (No. of colonies/No. of seeded cells) × 100%.

2.14 | Transwell assays

Briefly, ccRCC cells and HLECs were starved for 24 h. Matrigel (#356234, dilution 1:8, Corning Inc., Corning, NY, USA) was added to the upper chamber of the Transwell plate (#REF3422, Corning Inc.). Subsequently, cells were seeded in the upper chamber (10^5 cells/chamber). Following overnight incubation, methanol was used to fix cells that invaded the upper chamber membrane. The subsequent steps involved staining the cells with 0.05% crystal violet and capturing random photographs. Additionally, Transwell chambers lacking Matrigel coating were utilized to assess the migration ability of the cells.

2.15 | Immunohistochemistry (IHC)

IHC assessments were conducted on tissues sourced from subcutaneous tumor models and patients. Concisely, tissues underwent fixation using 4% paraformaldehyde, followed by dehydration, paraffin embedding, sectioning, deparaffinization, and rehydration. Afterward, serial sections from tissues were incubated with primary antibodies along with their corresponding secondary antibodies. The Leica microscope was employed for capturing random section images. IHC score for the protein was calculated by three pathologists based on the followings: IHC score = protein staining intensity (0 = negative staining; 1 = weak staining; 2 = moderate staining; 3 = strong staining) × percentage of positive cells (0 = 0%; 1 = 1%-25%; 2 = 26%-50%; 3 = 51%-75%; 4 = 76%-100%). All patients provided written informed consent for the utilization of tissue samples. The list of antibodies is provided in Supplementary Table S2.

2.16 | Flow cytometry apoptosis assay

ccRCC cells underwent apoptosis analysis by a flow cytometer (Becton Dickinson, Franklin Lakes, NJ, USA) following staining with Annexin V-Phycoerythrin (PE) and 7-amino-actinomycin D (7-AAD) (#A213-01, Vazyme). Distinct combinations of 7-AAD and PE were applied to distinguish apoptosis at various stages. Subsequent analysis of the results was conducted using the FlowJo software (Becton Dickinson).

2.17 | Immunofluorescence

ccRCC cells were seeded onto circular coverslips (Biosharp) at a density of 10^5 cells per coverslip. Following a PBS rinse, the cells underwent fixation with formaldehyde (4%) for 10 min and permeabilization with Triton X-100 (0.5%) for 20 min. Subsequently, the coverslips were subjected to incubation at 4°C for 24 h with primary antibodies, followed by treatment with fluorescence secondary antibody at room temperature for 2 h. Nuclei staining was accomplished with 4',6-diamidino-2-phenylindole (DAPI) (#C1002, Beyotime) for 30 min at room temperature, followed by image capture utilizing the Leica microscope. The list of antibodies is provided in Supplementary Table S2.

2.18 | Subcellular fractionation

The separation of nuclear and cytoplasmic proteins in ccRCC cells was accomplished using the nucleocytoplasmic separation kit (#P0028, Beyotime). Subsequently, Western blotting assays were conducted to detect proteins in the nuclear and cytoplasmic fractions.

2.19 | Mass spectrometry (MS) analysis

MS analyses were carried out by GeneChem. Briefly, gel strips were obtained through the electrophoresis of magnetic immune complexes from co-IP assays. Subsequently, protein gel strips underwent a series of sequential processes, including decolorization, alkylation, enzymatic hydrolysis, extraction, and desalination to yield peptide samples. These peptide samples were subjected to the TOF 5600 LC/MS system (AB SCIEX, Framingham, MA, USA). Original MS/MS files were then submitted to ProteinPilot (Version 4.5, SCIEX, Redwood, CA, USA) for comprehensive data analysis. For protein identification, the Paragon algorithm was utilized to search the Uniprot database (https://www.uniprot.org/). Peptides with an unused score > 1.3 (credibility exceeding 95%) were acknowledged as credible peptides.

2.20 | Bioinformatics and statistical analyses

Public RNA-seq data of ccRCC were obtained from The Cancer Genome Atlas (TCGA-KIRC, https://portal.gdc.cancer.gov) and the International Cancer Genome Consortium databases (ICGC-RECA, https://dcc.icgc.org/). Public proteomic data of ccRCC were obtained from the Clinical Proteomic Tumor Analysis Consortium (CPTAC3, https://registry.opendata.aws/cptac-3). The DESeq2 package (R Core Team, https://www.r-project.org) was used to identify differentially expressed genes (DEGs). The criteria of DEGs were adjusted $P < 0.05$ and |log fold-change| >1.5. Kaplan-Meier analyses were used to explore the associations between the overall survival rates and the mRNA levels of *NAT10* and *ANKZF1*. Survival duration was determined starting from the initial pathological diagnosis of ccRCC and extended until either death from any cause or the latest follow-up. Patients were categorized into low and high subgroups using median expression (50%) as the cut-off. Functional enrichment analyses were carried out through Gene Set Enrichment Analysis (GSEA) and Kyoto Encyclopedia of Genes and Genomes (KEGG) analysis in R software (R Core Team).

Statistical analysis was conducted using GraphPad 9.0 (San Diego, CA, USA) and SPSS 26.0 (IBM Corporation, Armonk, NY, USA). Student's *t*-test, Wilcoxon test, Mann-Whitney test, Spearman correlation, analysis of variance (ANOVA), Kruskal-Wallis test, and log-rank test were conducted. Assays were performed at least three times.

3 | RESULTS

3.1 | NAT10 catalyzed ac^{4}C modifications and was upregulated in ccRCC

Although prior studies have highlighted the significance of ac^{4}C in tumor progression [28, 29], its function in ccRCC has never been reported. Here, we found an increased ac^{4}C modification level of total mRNA in ccRCC tissues when compared with mRNA from adjacent normal tissues (Figure 1A). Then, the dot blotting and colorimetric assays both indicated that ccRCC cells presented stronger ac^{4}C levels than the control RPTECs (Figure 1B and Supplementary Figure S1A). Since, in all cases, ac^{4}C production has been catalyzed by NAT10 [26], this study next evaluated the expression levels of NAT10 in ccRCC. Data from the public databases (TCGA-KIRC and ICGC-RECA) showed that *NAT10* was upregulated in ccRCC (Figure 1C), and the protein expression of NAT10 also increased in the CPTAC3-ccRCC database (Figure 1D). More than that, Western blotting and qPCR assays found that NAT10 was upregulated in ccRCC cell lines (Figure 1E-F) and ccRCC tissues (Supplementary Figure S1B-C). Meanwhile, IHC staining revealed an increased level of NAT10 in tumor tissues compared with adjacent normal tissues (Figure 1G-H). To confirm that ac^{4}C modification in ccRCC is catalyzed by NAT10, we established NAT10-overexpressed and NAT10-knockdown ccRCC cells (Supplementary Figure S1D-E). Dot blotting and colorimetric assays both showed that ccRCC cells with NAT10 overexpression had elevated ac^{4}C levels in total mRNA while NAT10-knockdown ccRCC cells exhibited decreased ac^{4}C levels when compared with the control cells (Figure 1I-J and Supplementary Figure S1F-G). These results suggested that the expression level of NAT10 was elevated and NAT10 functioned as a "writer" of ac^{4}C in ccRCC.

3.2 | NAT10 promoted tumor progression in ccRCC

To explore the roles of NAT10 in the development of ccRCC, we conducted cell viability assays. It was presented that NAT10-overexpressed ccRCC cells exhibited strengthened viabilities compared with the control cells;

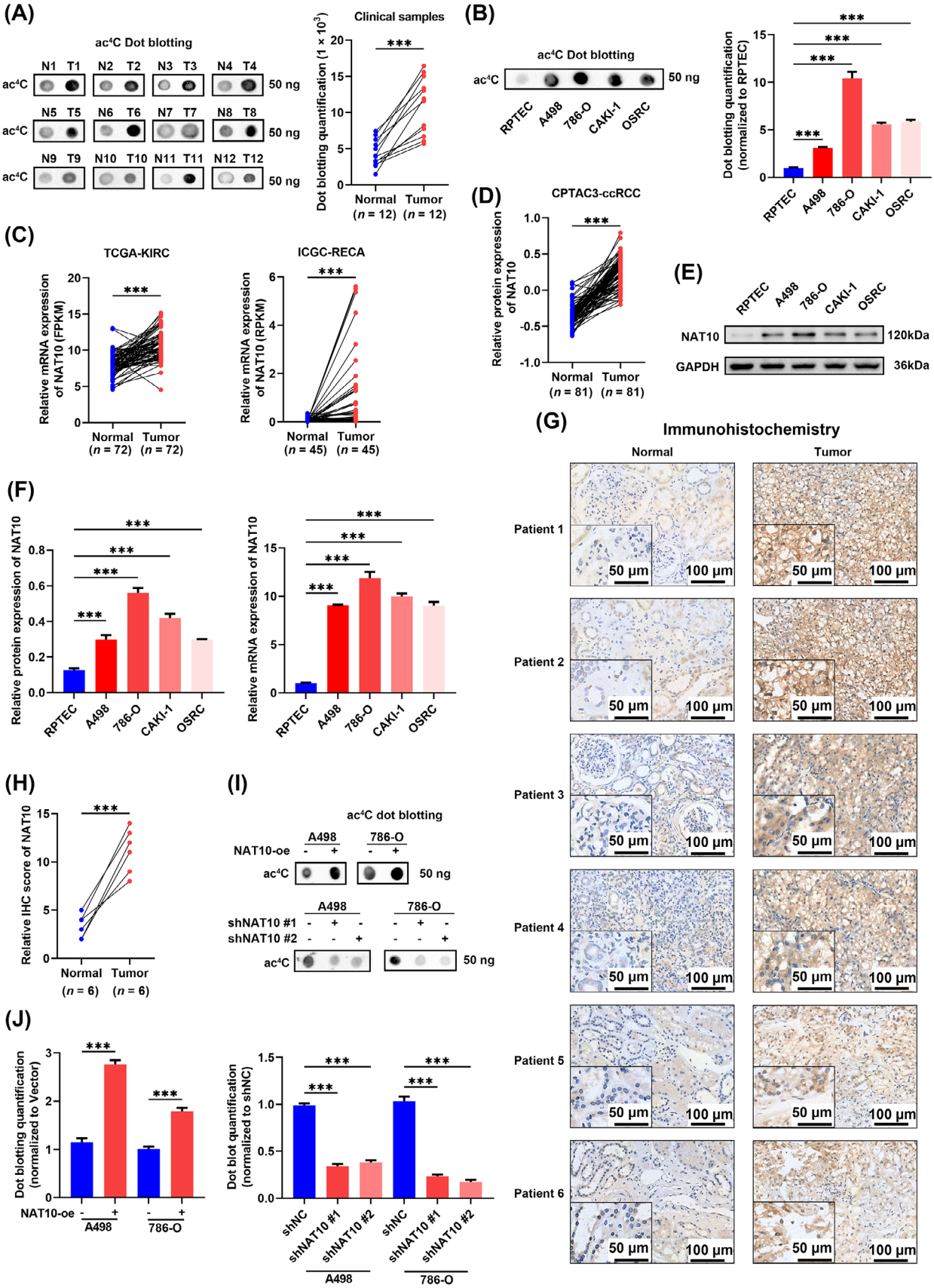

FIGURE 1 NAT10 catalyzed ac^{4}C modifications and was upregulated in ccRCC. (A) Anti-ac^{4}C dot blotting of total mRNA from ccRCC tissues and adjacent normal tissues. The loading amount of each sample was fixed to 50 ng mRNA ($n = 12$) (t-test for statistics). (B) Anti-ac^{4}C dot blotting of total mRNA from cell lines. The loading amount of each sample was fixed to 50 ng mRNA ($n = 3$) (ANOVA for statistics). The

on the contrary, ccRCC cells with NAT10 knockdown exhibited decreased viabilities (Supplementary Figure S2A). Colony formation assays indicated that NAT10-knockdown ccRCC cells exhibited decreased abilities of proliferation (Figure 2A). Transwell assays denoted that ccRCC cells with NAT10 overexpression presented enhanced abilities of migration and invasion (Figure 2B and Supplementary Figure S2B). Concurrently, the migration and invasion ability of NAT10-knockdown ccRCC cells was reduced (Supplementary Figure S2C-D). Moreover, apoptotic rates decreased in NAT10-overexpressed ccRCC cells and significantly increased in ccRCC cells with NAT10 knockdown (Figure 2C and Supplementary Figure S2E). After reintroducing NAT10 in NAT10-knockdown cells (Supplementary Figure S3A), we observed a restoration in cell proliferation, invasion, migration, and anti-apoptotic abilities (Supplementary Figure S3B-D). Then CAKI-1 cells were injected into 5-week-old BALB/c nude mice. The volume and weight of subcutaneous tumors from the NAT10-knockdown group were reduced compared with the control group (Figure 2D). In addition, the expression of Ki67 (the marker of cellular proliferation) also decreased in the NAT10-knockdown group (Figure 2E-F). Small animal fluorescent imaging assays suggested that mice injected with NAT10-knockdown ccRCC cells exhibited decreased abilities of tumor metastasis (Figure 2G). The above findings suggested that NAT10 played a critical role in the progression of ccRCC.

3.3 | NAT10 promoted tumor lymphangiogenesis in ccRCC

Remarkably, tumor lymphangiogenesis is indispensable for the development and progression of various cancers [10, 32, 33]. In the case of ccRCC, lymphangiogenesis demonstrated a close relationship with lymphatic metastasis and patient survival [19–21]. To explore whether NAT10 regulated tumor lymphangiogenesis in ccRCC, we first conducted GSEA based on the TCGA-KIRC dataset with NAT10-high versus NAT10-low tumors. The results presented that NAT10 was involved in tumor lymphangiogenesis via the VEGF signaling (Figure 3A). Then we assessed the effect of NAT10 on HLECs by proliferation and migration assays. HLECs were cultured with the CM derived from ccRCC cells. The cell viability assays showed that overexpression of NAT10 in ccRCC cells increased the viability of HLECs (Figure 3B), while knockdown of NAT10 inhibited the viability of HLECs (Figure 3C). Transwell assays indicated that overexpression of NAT10 in ccRCC cells improved the migration ability of HLECs (Figure 3D). Concurrently, the migration ability of HLECs was significantly reduced when cultured with CM from NAT10-knockdown ccRCC cells (Figure 3E). Moreover, tube formation assays indicated that overexpression of NAT10 in ccRCC cells efficiently enhanced lymphangiogenesis in vitro (Figure 3F and Supplementary Figure S4A), and the depletion of NAT10 inhibited tube formation of HLECs (Figure 3G and Supplementary Figure S4B). Then ELISAs were applied to detect the concentrations of VEGFC/D in the CM from ccRCC cells. It was presented that overexpression of NAT10 promoted the secretion of VEGFC/D in A498 and 786-O cells, while cells with NAT10 knockdown exhibited a decreased section of VEGFC/D (Figure 3H and Supplementary Figure S4C). Subsequently, we assessed the mRNA levels of *VEGFC/D* in ccRCC cells. Notably, NAT10 was observed to induce an elevation in the mRNA levels of *VEGFC/D* (Supplementary Figure S4D). To further confirm the role of VEGFC/D in mediating NAT10-induced lymphangiogenesis, we employed siRNA targeting *VEGFR3* (VEGFC/D receptors) in HLECs. The results showed that VEGFR3-knockdown HLECs effectively counteracted the pro-lymphangiogenic effect induced by NAT10 overexpression (Supplementary Figure S4E-I). In addition, we found that the expression level of VEGFC/D was significantly reduced in the NAT10-knockdown subcutaneous tumors (Figure 3I). IHC staining results of lymphatic vessel endothelial hyaluronan receptor 1 (LYVE1) revealed that lymphatic vessel density decreased with NAT10 knockdown (Figure 3I). The above findings indicated that NAT10 was a pro-lymphangiogenic factor of ccRCC.

quantification results were normalized to the control cells. (C) The mRNA levels of *NAT10* in ccRCC tissues and paired adjacent normal tissues based on TCGA-KIRC and ICGC-RECA (Wilcoxon test for statistics). (D) The protein level of NAT10 in ccRCC tissues and paired adjacent normal tissues based on the CPTAC3-ccRCC database (*t*-test for statistics). (E-F) Protein and mRNA levels of NAT10 in cell lines ($n = 3$) (ANOVA for statistics). (G-H) Representative IHC staining images for NAT10 in ccRCC tissues and adjacent normal tissues ($n = 6$) (Mann-Whitney U test for statistics). (I-J) Anti-ac^{4}C dot blotting of total mRNA from A498 and 786-O cells with NAT10 overexpression or knockdown ($n = 3$) (*t*-test and ANOVA for statistics). The quantification results were normalized to the control cells. Results represented at least three independent experiments (*$P < 0.05$, **$P < 0.01$, ***$P < 0.001$). Abbreviations: NAT10, N-acetyltransferase 10; ccRCC, clear-cell renal cell carcinoma; ac^{4}C, N4-acetylcytidine; TCGA, the cancer genome atlas; KIRC, kidney renal clear-cell carcinoma; ICGC-RECA, the international cancer genome consortium-renal cancer; CPTAC3, clinical proteomic tumor analysis consortium 3; IHC, immunohistochemical; FPKM, fragments per kilobase of exon model per million mapped fragments; RPKM, reads per kilobase per million mapped reads; GAPDH, glyceraldehyde-3-phosphate dehydrogenase.

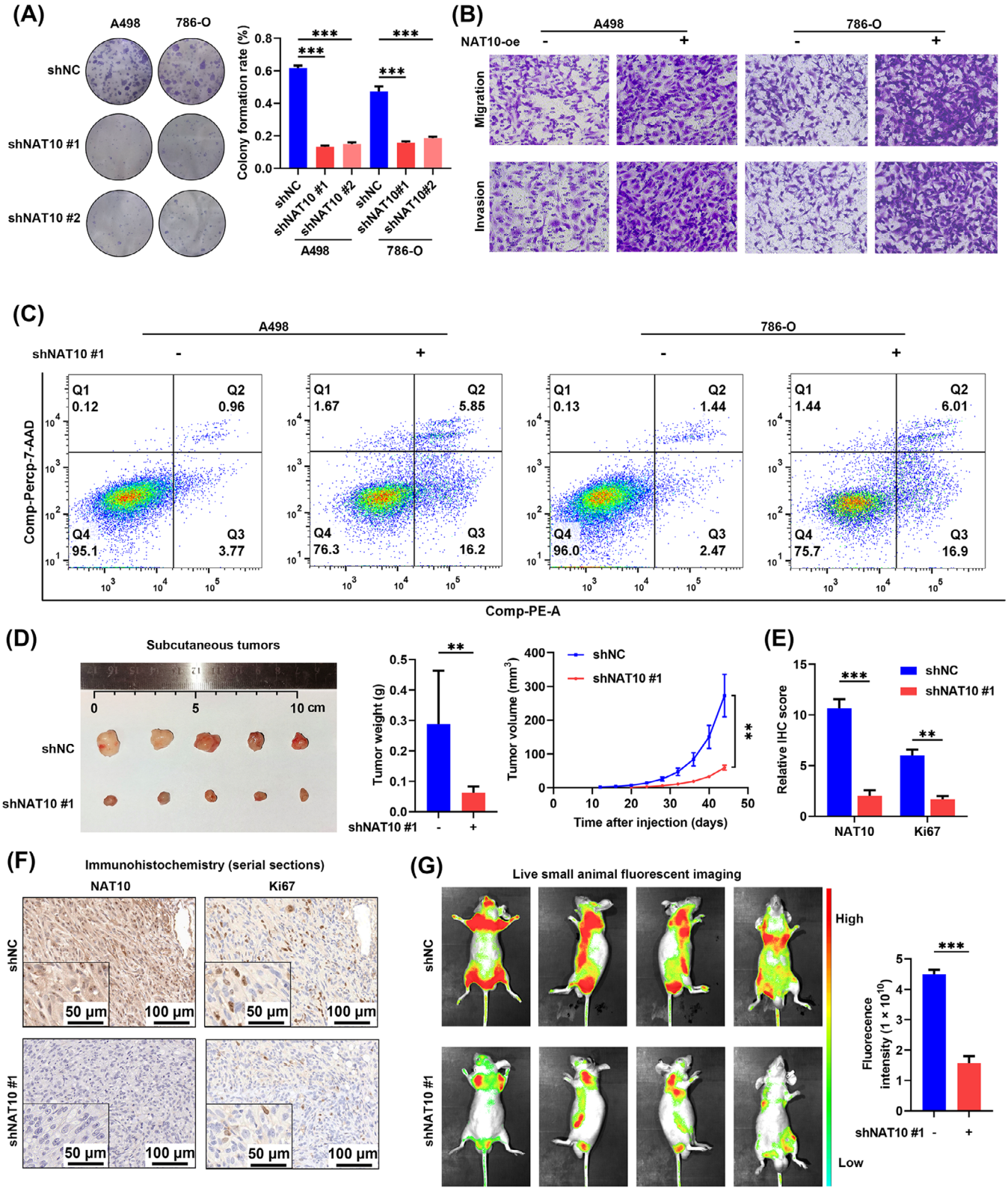

FIGURE 2 NAT10 promoted tumor progression in ccRCC. (A) Colony formation assays for the NAT10-knockdown ccRCC cells and the control cells ($n = 3$) (ANOVA for statistics). (B) Transwell assays for the NAT10-overexpressed ccRCC cells or the control cells ($n = 3$). (C) Flow cytometry assays showed the proportion of apoptotic cells in NAT10-knockdown ccRCC cells and the control cells ($n = 3$). Comp-PE-A means Annexin V was compensated by negative control and single positive control. Comp-Percp-7-AAD means 7-AAD was compensated by negative control and single positive control. (D) CAKI-1 cells with NAT10 knockdown were injected into nude mice. Tumors were extracted after mice were euthanized ($n = 5$) (*t*-test for statistics). (E-F) IHC of NAT10 and Ki67 in subcutaneous tumors from the NAT10-knockdown group and the control group ($n = 5$) (Mann-Whitney U test for statistics). (G) Live small animal fluorescent images of the metastasis model in

3.4 | NAT10 promoted tumor progression and lymphangiogenesis in ccRCC by enhancing the nuclear localization of YAP1

To elucidate the mechanisms by which NAT10 promoted tumor progression and lymphangiogenesis in ccRCC, this study performed RNA-seq analysis in ccRCC cells after NAT10 silencing (Supplementary Figure S5A). KEGG pathway enrichment analysis indicated that Hippo signaling was the dominant pathway among the functional enrichment results (Supplementary Figure S5B). We also observed differential mRNA levels in several established targets of the Hippo signaling [34] between the NAT10-knockdown and control groups (Supplementary Figure S5C). Subsequently, we found that two common makers of Hippo signaling, connective tissue growth factor (*CTGF*) and cysteine-rich 61 (*CYR61*), were downregulated in NAT10-knockdown ccRCC cells (Supplementary Figure S5D). Moreover, *CTGF* and *CYR61* were upregulated in NAT10-overexpressed ccRCC cells (Supplementary Figure S5E). However, the mRNA level of *YAP1*, the core effector of Hippo signaling, has no statistical difference upon NAT10 knockdown or overexpression (Supplementary Figure S5D-E). Western blotting showed that the overexpression or knockdown of NAT10 did not influence the protein level of phosphorylated or total YAP1 either (Supplementary Figure S5F-G). Since YAP1 dynamically shuttles between the cytoplasm and the nucleus where it acts as an activator of gene transcription, this study next conducted a series of nucleocytoplasmic separation assays. It was demonstrated that NAT10-knockdown ccRCC cells inhibited YAP1 nuclear localization (Figure 4A), while NAT10-overexpressed ccRCC cells inhibited cytoplasmic localization of YAP1 (Supplementary Figure S6A). Immunofluorescence assays showed that NAT10 overexpression elevated the translocation of YAP1 into the nucleus (Figure 4B), while NAT10 knockdown reduced the nuclear YAP1 staining (Supplementary Figure S6B). Upon the reintroduction of NAT10 into NAT10-knockdown ccRCC cells, a significant increase in YAP1 nuclear localization was observed (Supplementary Figure S6C). Given the influence of classical regulators large tumor suppressor kinase 1/2 (LATS1/2) and moesin-ezrin-radixin like tumor suppressor (NF2) on YAP1 localization [35], we explored whether NAT10-mediated YAP1 nuclear translocation is also affected by LATS1/2 and NF2. The nucleocytoplasmic separation assays indicated that the knockdown of LATS1 or NF2 partially alleviated the cytoplasmic retention of YAP1 induced by NAT10 depletion (Supplementary Figure S7A-B). These results suggested that NAT10-mediated nuclear translocation of YAP1 was partially dependent on the classical phosphorylation pathway. To examine whether the Hippo pathway is critical in NAT10-mediated tumor promotion and lymphangiogenesis, the siRNA targeting *YAP1* was applied to treat NAT10-overexpressed ccRCC cells. Cell viability assays indicated that the knockdown of YAP1 alleviated the promotion of proliferation by NAT10 overexpression (Figure 4C). Moreover, the knockdown of YAP1 offset the promotion of invasion and migration driven by NAT10 overexpression (Supplementary Figure S7C). The knockdown of YAP1 also rescued the apoptosis-resistant phenotype caused by the overexpression of NAT10 (Supplementary Figure S8A-B). These data confirmed that NAT10 repressed the non-canonical Hippo signaling and then promoted tumor progression in ccRCC.

Next, we found that the knockdown of YAP1 offset the promotion of tumor lymphangiogenesis caused by NAT10 overexpression (Figure 4D-E and Supplementary Figure S8C-D). To investigate the mechanisms underlying the tube formation of HLECs cultured in CM from ccRCC cells, RNA-seq data from shNC/shNAT10 and siNC/siYAP1 groups were analyzed to draw a Venn diagram (Supplementary Figure S9A). Subsequently, the mRNA levels of the six candidates were measured in the ccRCC cells with YAP1 knockdown. The results showed that the mRNA levels of both *VEGFC/D* decreased significantly after YAP1 knockdown (Supplementary Figure S9B). Moreover, the protein levels of VEGFC/D increased in NAT10-overexpressed ccRCC cells and decreased in NAT10-knockdown ccRCC cells (Figure 4F and Supplementary Figure S9C-D). Western blotting showed that the knockdown of YAP1 alleviated the increased expression of VEGFC/D in NAT10-overexpressed ccRCC cells (Figure 4G and Supplementary Figure S9E). These results supported that NAT10 promoted tumor lymphangiogenesis by upregulating the expression levels of VEGFC/D.

3.5 | ANKZF1 was identified as a functional target of NAT10 in ccRCC

To investigate the potential targets regulated by NAT10 in ccRCC, RNA-seq and NAT10-RIP-seq data were analyzed

the NAT10-knockdown group and control group. The images depict one mouse from each group in four distinct body positions. Nude mice were imaged eight weeks after performing tail vein injections of A498 cells ($n = 5$) (*t*-test for statistics). Results represented at least three independent experiments (*$P < 0.05$, **$P < 0.01$, ***$P < 0.001$). Abbreviations: NAT10, N-acetyltransferase 10; ccRCC, clear-cell renal cell carcinoma; PE, phycoerythrin; 7-AAD, 7-amino-actinomycin D; IHC, immunohistochemical; Ki-67, marker of proliferation ki-67.

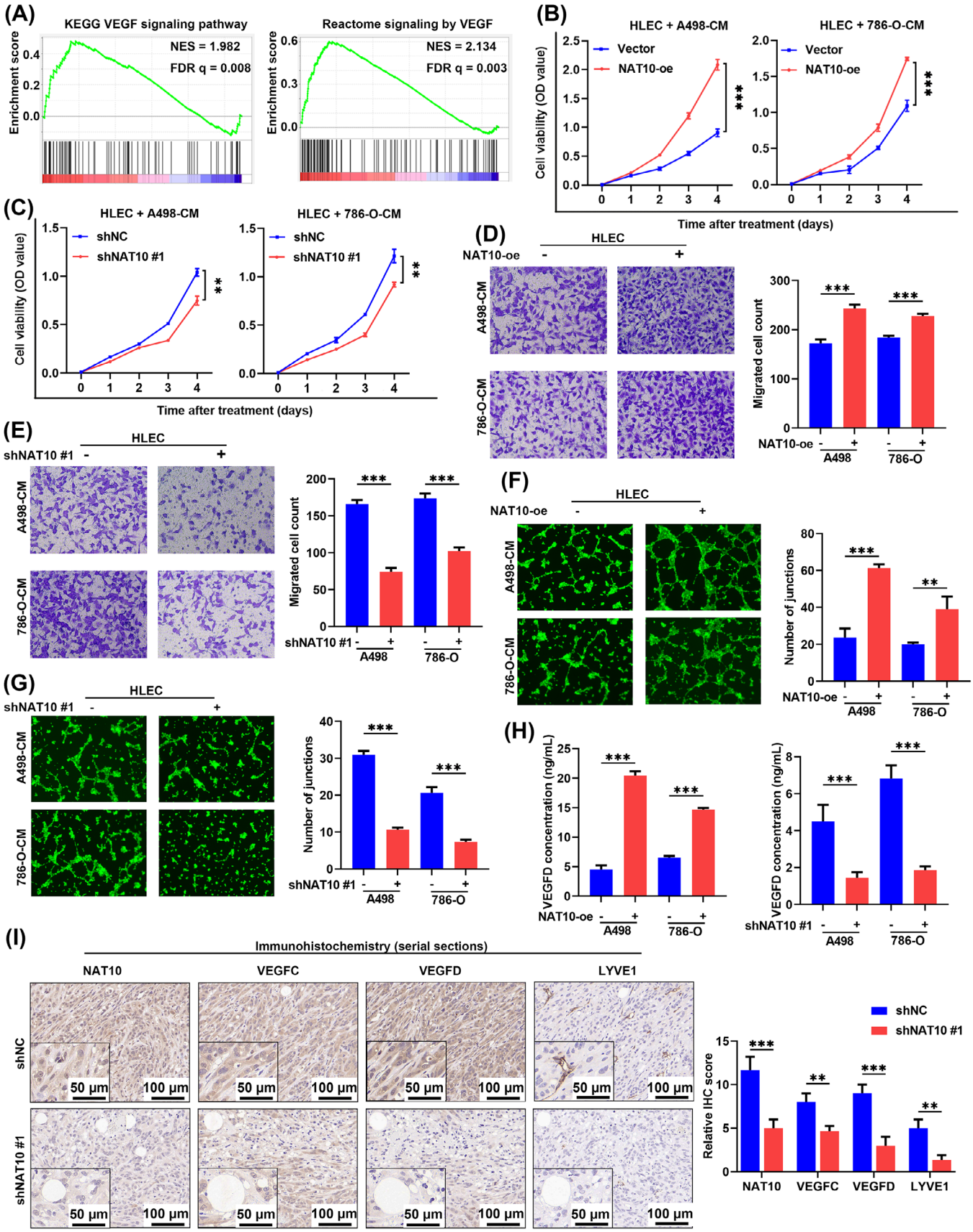

FIGURE 3 NAT10 promoted tumor lymphangiogenesis in ccRCC. (A) GSEA showed the associations between the VEGF signaling and the *NAT10* mRNA levels in ccRCC. FDR q < 25% was considered statistically significant. Patients were categorized into low and high subgroups using median expression (50%) as the cut-off. (B) Cell proliferation curves of HLECs treated with CM from the NAT10-overexpressed ccRCC cells and the control cells ($n = 4$) (t-test for statistics). (C) Cell proliferation curves of HLECs treated with CM

together to draw a Venn diagram (Figure 5A). It was displayed that NAT10 bound to 2,395 mRNAs, among which ANKZF1 were simultaneously downregulated upon NAT10 knockdown and most closely correlated with NAT10 in the TCGA-KIRC database (Figure 5A and Supplementary Figure S10A). Hence, this study hypothesized that the expression of ANKZF1 was regulated by NAT10-mediated ac^{4}C modification. To further validate our hypothesis, ac^{4}C-RIP-qPCR assays were performed. It was found that ac^{4}C abundances of *ANKZF1* increased in tumor tissues and cell lines of ccRCC (Figure 5B-C), in which the levels of NAT10-mediated ac^{4}C modification were previously proved to be elevated in the present study. Moreover, NAT10 overexpression enhanced the ac^{4}C modification in the *ANKZF1* mRNA in A498 and 786-O cells (Figure 5D). On the contrary, the ac^{4}C abundances of *ANKZF1* were reduced upon NAT10 knockdown (Supplementary Figure S10B). Subsequently, the mRNA half-life assay demonstrated that the stability of *ANKZF1* was significantly enhanced by NAT10 upregulation (Figure 5E). On the contrary, NAT10 reduction reduced the stability of *ANKZF1* mRNA (Figure 5E). Similarly, mRNA levels of *ANKZF1* markedly increased after NAT10 overexpression and decreased after NAT10 knockdown (Supplementary Figure S10C-D). The ANKZF1 protein expression increased after NAT10 overexpression and decreased after NAT10 knockdown (Figure 5F and Supplementary Figure S10E). These results denoted the NAT10-mediated ac^{4}C modification raised the expression of ANKZF1 in ccRCC.

To confirm the biological function of ANKZF1 in ccRCC, ccRCC cells with ANKZF1 knockdown were established (Supplementary Figure S10F-G). Cell viability assays presented that the ccRCC cells with ANKZF1 knockdown exhibited decreased proliferation ability (Supplementary Figure S10H). Transwell assays denoted that the migration and invasion abilities of ANKZF1-knockdown ccRCC cells were reduced (Supplementary Figure S10I). To confirm the biological relevance of ANKZF1 in mediating NAT10-regulated ccRCC progression, rescue experiments were performed by reintroducing ANKZF1 to NAT10-knockdown ccRCC cells. Cell viability assays indicated that overexpression of ANKZF1 enhanced the proliferation ability of NAT10-knockdown ccRCC cells (Supplementary Figure S11A). Similarly, overexpression of ANKZF1 rescued the decreased migration and invasion capacity after the knockdown of NAT10 (Supplementary Figure S11B). The increased apoptotic rates induced by the knockdown of NAT10 were also reduced by overexpression of ANKZF1 in ccRCC cells (Figure 5G and Supplementary Figure S11C). Moreover, we found that overexpression of ANKZF1 offset the anti-lymphangiogenic effect caused by the knockdown of NAT10 (Figure 5H-I and Supplementary Figure S12A-B). Additionally, Western blotting showed that overexpression of ANKZF1 rescued the downregulation of VEGFC/D in the NAT10-knockdown ccRCC cells (Figure 5J and Supplementary Figure S12C). Similarly, the knockdown of ANKZF1 resulted in a reduction in the upregulation of VEGFC/D in NAT10-overexpressed ccRCC cells (Supplementary Figure S12D). Together, these findings demonstrated that NAT10-dependent ac^{4}C modification of *ANKZF1* functionally regulated the biological processes of ccRCC cells.

3.6 | NAT10 inactivated the non-canonical Hippo signaling by enhancing the ANKZF1-YWHAE interaction

The previous findings of this study suggested that NAT10 functioned as an oncogene in ccRCC by silencing non-canonical Hippo signaling or by upregulating ANKZF1. These findings hinted at a link between ANKZF1 and the non-canonical Hippo pathway. To explore the effect of ANKZF1 on the non-canonical Hippo signaling in ccRCC, YAP1 and phosphorylated YAP1 abundances in ccRCC cells were measured. It was demonstrated that overexpression or knockdown of ANKZF1 presented no significant effect on YAP1 at the protein expression (Supplementary Figure S13A-B). However, nucleocytoplasmic

from the NAT10-knockdown ccRCC cells and the control cells ($n = 4$) (t-test for statistics). (D) Transwell assays for HLECs treated with CM from the NAT10-overexpressed ccRCC cells and the control cells ($n = 3$) (t-test for statistics). (E) Transwell assays for HLECs treated with CM from the NAT10-knockdown ccRCC cells and the control cells ($n = 3$) (t-test for statistics). (F) Tube formation assays for HLECs treated with CM from the NAT10-overexpressed ccRCC cells and the control cells ($n = 3$) (t-test for statistics). (G) Tube formation assays for HLECs treated with CM from the NAT10-knockdown ccRCC cells and the control cells ($n = 3$) (t-test for statistics). (H) ELISAs were used to detect the VEGFD concentrations in CM from ccRCC cells with NAT10 overexpression or knockdown ($n = 3$) (t-test for statistics). (I) IHC of NAT10, VEGFC/D, and LYVE1 in subcutaneous tumors from the NAT10-knockdown group and the control group ($n = 5$) (Mann-Whitney U for statistics). Results represented at least three independent experiments (*$P < 0.05$, **$P < 0.01$, ***$P < 0.001$). Abbreviations: NAT10, N-acetyltransferase 10; ccRCC, clear-cell renal cell carcinoma; GSEA, gene set enrichment analysis; FDR, false discovery rate; NES, normalized enrichment score; VEGF, vascular endothelial growth factor; HLEC, human lymphatic endothelial cell; CM, conditioned medium; ELISA, Enzyme-linked immunosorbent assay; VEGFC/D, vascular endothelial growth factor-C/D; LYVE1, lymphatic vessel endothelial hyaluronan receptor 1; KEGG, kyoto encyclopedia of genes and genomes.

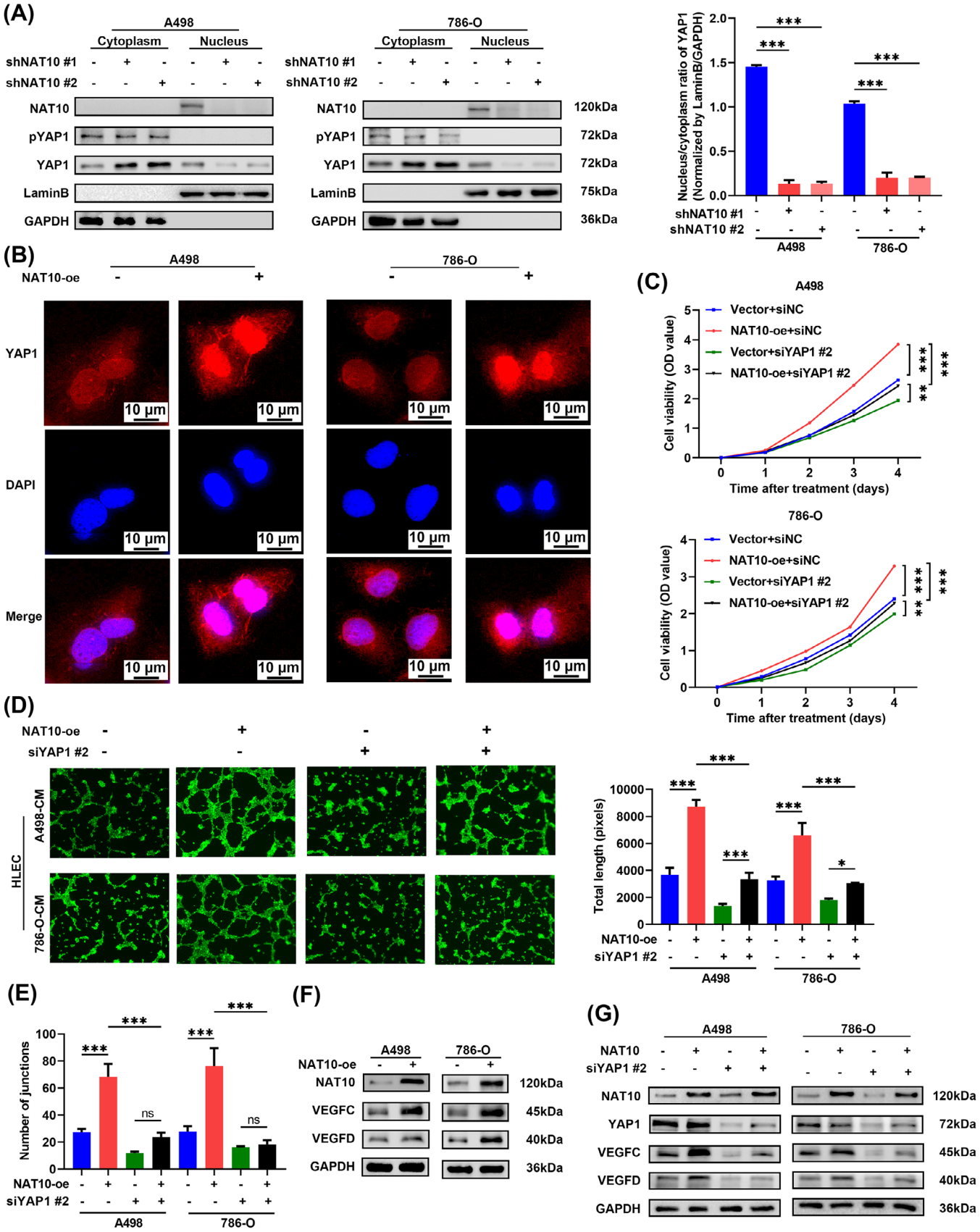

FIGURE 4 NAT10 promoted tumor progression and lymphangiogenesis in ccRCC by enhancing the nuclear localization of YAP1. (A) Western blotting showed the subcellular localization of YAP1 after NAT10 knockdown ($n = 3$) (ANOVA for statistics). (B) Immunofluorescence assays displayed subcellular localization of YAP1 after NAT10 overexpression. (C) Cell proliferation curves of cell viability assays for the

separation assays indicated that ANKZF1 altered YAP1 nuclear-cytoplasmic localization in ccRCC (Figure 6A and Supplementary Figure S13C). These data supported that ANKZF1 inactivated non-canonical Hippo signaling, resulting in the nuclear localization of YAP1. To clarify how ANKZF1 affected the nuclear-cytoplasmic localization of YAP1, IP/MS experiments were conducted in this study. Briefly, Flag-ANKZF1 or vector was reintroduced in HEK293T cells (Supplementary Figure S13D-E), and IP followed by MS analyses was performed. We found that 354 proteins were pulled down by Flag-ANKZF1, not by the vector. Among these proteins, 5 candidates were also included in the Hippo-associated proteins from the KEGG database (Figure 6B). Among these candidates, YWHAE was reported to interact with YAP1 in various cancers, leading to the cytoplasmic localization of YAP1 [36]. To validate whether YWHAE could inhibit the transcriptional activation of YAP1 in ccRCC, this study assessed the mRNA level of known target genes of the Hippo signaling in YWHAE-overexpressed cells. The results revealed a significant downregulation of *CTGF* and *CYR61* upon YWHAE overexpression, suggesting a decrease in the transcriptional activity of YAP1 (Supplementary Figure S13F). Conversely, mRNA levels of *CTGF* and *CYR61* were markedly upregulated in YWHAE-knockdown ccRCC cells (Supplementary Figure S13G). This study further found that YWHAE-knockdown ccRCC cells displayed increased abilities for proliferation, invasion, and migration (Supplementary Figure S14A-C). Additionally, a notable reduction in the rate of apoptosis was observed (Supplementary Figure S14D-E). Moreover, the knockdown of YWHAE restored the tumor-suppressive effects caused by NAT10 knockdown (Supplementary Figure S14).

Subsequently, co-IP assays were conducted to explore how ANKZF1/YWHAE regulated the non-canonical Hippo signaling. We found that, in HEK293T cells, endogenous ANKZF1 and YWHAE were efficiently immunoprecipitating with each other (Figure 6C). Further to confirm this interaction, Myc-YWHAE and Flag-ANKZF1 were reintroduced in HEK293T cells. It was observed that, in HEK293T cells, Flag-ANKZF1 and Myc-YWHAE interacted with each other (Figure 6D). Next, we repeated co-IP assays in A498 and 786-O cells, the results of which denoted that Flag-ANKZF1 and Myc-YWHAE bound to each other in ccRCC (Figure 6E). This study next sought to define whether the overexpression or knockdown of ANKZF1 could affect the interaction between YWHAE and YAP1 or not. In ANKZF1-overexpressed A498 and 786-O cells, YWHAE immunoprecipitated fewer YAP1 proteins (Figure 6F). On the contrary, the depletion of ANKZF1 commanded more interaction between YWHAE and YAP1 (Figure 6G). Furthermore, this study found that in NAT10-overexpressed ccRCC cells, there was an upregulation of ANKZF1, accompanied by a reduced binding of YWHAE to YAP1 (Supplementary Figure S15A). Conversely, upon NAT10 knockdown, the expression of ANKZF1 was downregulated, resulting in increased interaction between YWHAE and YAP1 (Supplementary Figure S15B). Given the phosphorylation-dependent interaction between YWHAE and YAP1 at the S127 site [36], this study introduced plasmids carrying YAP1 mutations (S127A and 5SA) into ccRCC cells and performed co-IP assays. The results indicated an enhanced binding affinity between YWHAE and the wild-type YAP1 (Supplementary Figure S15C). However, this interaction was notably impaired in the presence of YAP1 mutations at the S127A or 5SA site (Supplementary Figure S15C). Subsequent nucleocytoplasmic separation assays indicated that NAT10 specifically influenced the localization of wild-type YAP1 (Supplementary Figure S15D). Remarkably, both S127A and 5SA YAP1 mutants predominantly localized to the cell nucleus, and their intracellular distribution remained unaffected by the NAT10/ANKZF1 axis (Supplementary Figure S15D). Then five truncated plasmids of Flag-ANKZF1 were cloned and reintroduced to HEK293T cells (Figure 6H). Among all parts of Flag-ANKZF1, only Part 5 interacted with YWHAE (Figure 6I), suggesting that the amino acids between 600 and 726 in ANKZF1 were mandatory for its interaction with YWHAE. To confirm the role of YWHAE in mediating ANKZF1-induced nuclear localization of YAP1 in ccRCC, rescue experiments were performed by silencing YWHAE in ANKZF1-knockdown ccRCC cells. Western blotting showed that the knockdown of YWHAE did not influence the protein levels of phosphorylated or total YAP1 in ANKZF1-knockdown ccRCC cells (Supplementary Figure S15E-F), which was consistent with the previous findings. However, the nucleocytoplasmic separation assays indicated that the knockdown of YWHAE inhibited the cytoplasmic localization of YAP1 induced by ANKZF1 knockdown (Figure 6J and Supplementary

indicated ccRCC cells ($n = 4$) (ANOVA for statistics). (D-E) Tube formation assays for HLECs treated with CM from the indicated ccRCC cells ($n = 3$) (ANOVA for statistics). (F) The protein levels of VEGFC/D in ccRCC cells with NAT10 overexpression and the control cells. (G) The protein levels of NAT10, YAP1, and VEGFC/D in the indicated ccRCC cells. Results represented at least three independent experiments (*$P <$ 0.05, **$P < 0.01$, ***$P < 0.001$). Abbreviations: NAT10, N-acetyltransferase 10; ccRCC, clear-cell renal cell carcinoma; YAP1, yes1-associated transcriptional regulator; HLEC, human lymphatic endothelial cell; CM, conditioned medium; VEGFC/D, vascular endothelial growth factor-C/D; pYAP1, phosphorylated YAP1; GAPDH, glyceraldehyde-3-phosphate dehydrogenase; DAPI, 4',6-diamidino-2-phenylindole.

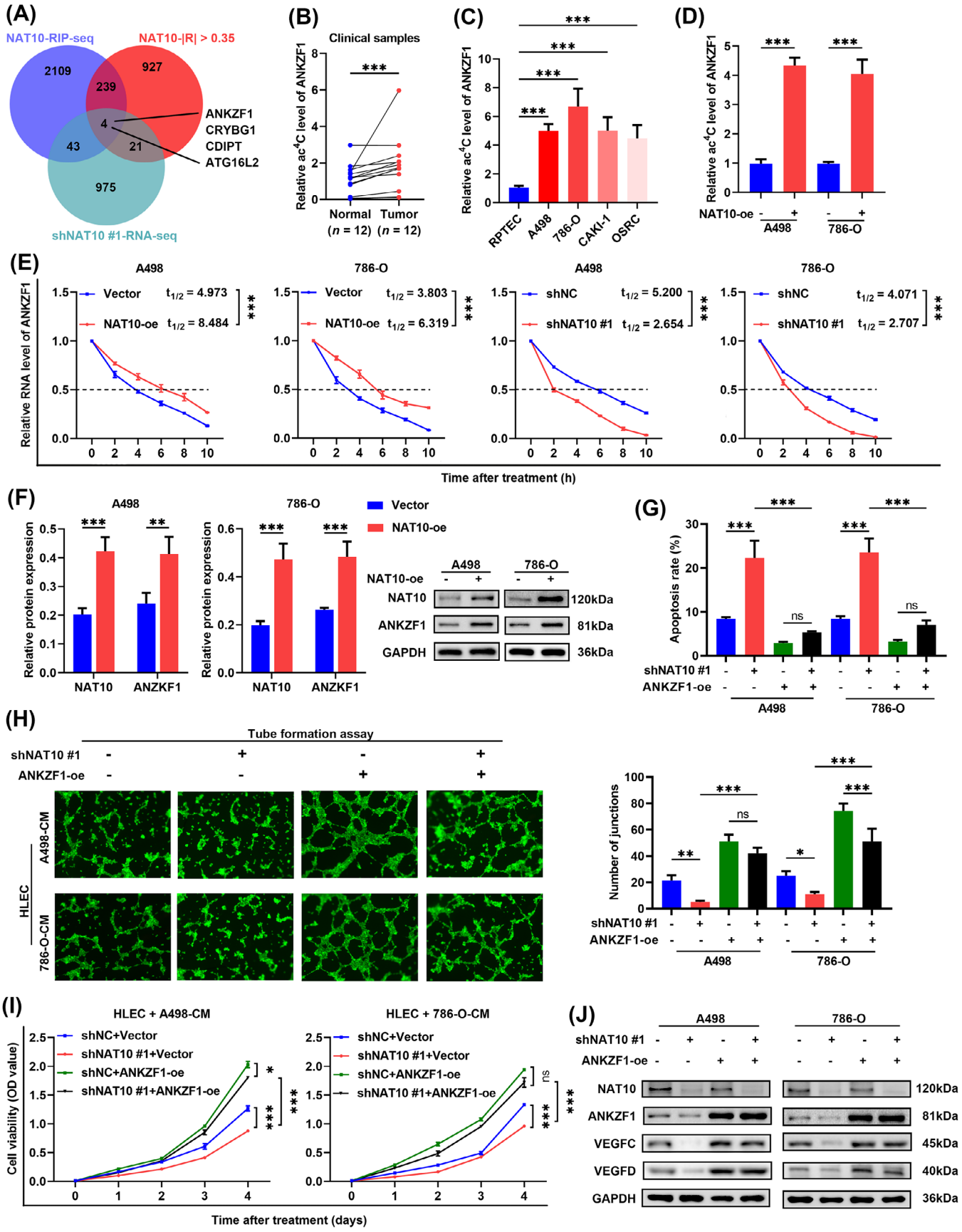

FIGURE 5 ANKZF1 was identified as a functional target of NAT10 in ccRCC. (A) Venn diagram of the downstream genes regulated by NAT10 in A498 ccRCC cells. "NAT10-RIP-seq" means that these genes were identified by NAT10-RIP-seq. "shNAT10-RNA-seq" means DEGs between the shNC and shNAT10 group. "NAT10-|R| > 0.35" means that the correlation between this gene set and NAT10 is greater than 0.35.

Figure S15G). These findings suggested that ANKZF1 directly interacted with YWHAE and inhibited the YWHAE-mediated cytoplasmic retention of YAP1.

3.7 | NAT10-ANKZF1 axis inactivated non-canonical Hippo signaling and suppressed ccRCC progression and lymphangiogenesis in vivo

The functions of YWHAE and ANKZF1 in NAT10-mediated YAP1 inhibition were investigated. We found that both overexpression of ANKZF1 and knockdown of YWHAE could eliminate the cytoplasmic localization of YAP1 driven by the knockdown of NAT10 (Supplementary Figure S16A-B). Interestingly, we observed that Tafazzin (TAZ), as a paralogue of YAP1, was also regulated by the NAT10/ANKZF1/YWHAE axis (Supplementary Figure S16A-B). Although overexpression of ANKZF1 or knockdown of YWHAE did not influence the level of total YAP1, they offset the effects of activating non-canonical Hippo signaling induced by knockdown of NAT10, resulting in elevated expression levels of VEGFC/D (Supplementary Figure S17). Next, the function of the NAT10/ANKZF1 axis was explored in vivo via animal models. Subcutaneous tumor models indicated that overexpression of ANKZF1 could reverse the growth inhibition induced by NAT10 knockdown (Figure 7A-C). IHC staining of subcutaneous tumors showed that the decreased expression levels of Ki67 and VEGFC/D in the NAT10-knockdown group were restored by the reintroduction of ANKZF1 (Figure 7D and Supplementary Figure S18A). IHC staining results of LYVE1 revealed that overexpression of ANKZF1 rescued the decreased lymphatic vessel density in the NAT10-knockdown group (Figure 7D and Supplementary Figure S18A). Immunofluorescence staining of subcutaneous tumors revealed that the reduced nuclear localization of YAP1/TAZ in the NAT10-knockdown group was partially restored upon the reintroduction of ANKZF1 (Supplementary Figure S18B-C). Small animal fluorescent imaging assays indicated that the overexpression of ANKZF1 reversed the inhibition of metastasis driven by NAT10 knockdown (Figure 7E and Supplementary Figure S18D). Also, the number of metastatic nodes in mouse livers was raised by the reintroduction of ANKZF1 for the NAT10-knockdown group (Supplementary Figure S18E). Finally, Kaplan-Meier analyses were conducted to assess the prognostic value of NAT10 and ANKZF1 for ccRCC patients based on the TCGA-KIRC cohort. The survival analyses showed that aberrant accumulation of either NAT10 or ANKZF1 was associated with poor overall survival of ccRCC patients (Figure 7F). Taken together, these observations suggested that the NA10T-ANKZF1 axis promoted tumor progression and lymphangiogenesis in ccRCC.

4 | DISCUSSION

Despite increasing evidence demonstrating that NAT10-mediated epigenetic ac^4C modification contributes to tumor development in several cancers [28, 29, 37], the function of NAT10 in ccRCC has not been identified. In the present study, we reported a pro-cancer role of NAT10 in ccRCC progression and lymphangiogenesis. ANKZF1, the functional downstream target of NAT10, interacted with YWHAE to competitively curb its transport function, leading to the increased nuclear import of YAP1 and transcription of *VEGFC/D* (Figure 8). Moreover, functional assays in vivo and in vitro validated that the NAT10-ANKZF1 axis accelerated malignant progression and lymphangiogenesis in ccRCC.

RNA modifications, termed epi-transcriptome, have gained sustained attention since their importance in RNA metabolism and gradually become a novel therapeutic target in various cancers [38–40]. ac^4C is one of the most

The list of candidates in the Venn diagram has been deposited in the Science Data Bank (www.scidb.cn). (B) The ac^4C modification levels of *ANKZF1* in ccRCC tissues and adjacent normal tissues ccRCC ($n = 12$) (Wilcoxon test for statistics). (C) The ac^4C modification levels of *ANKZF1* in ccRCC cell lines and the normal cell line ($n = 3$) (ANOVA for statistics). (D) The ac^4C modification levels of *ANKZF1* in NAT10-overexpressed ccRCC cells or the control cells ($n = 3$) (*t*-test for statistics). (E) The decay rate of *NAT10* mRNA after treatment with actinomycin D in A498 and 786-O cells with NAT10 knockdown or overexpression ($n = 3$) (*t*-test for statistics). (F) The protein expression of ANKZF1 in ccRCC cells with NAT10 overexpression ($n = 3$) (*t*-test for statistics). (G) The apoptosis rates of the indicated ccRCC cells from flow cytometry assays ($n = 3$) (ANOVA for statistics). (H) Tube formation assays for HLECs treated with CM from the indicated ccRCC cells ($n = 3$) (ANOVA for statistics). (I) Cell proliferation curves of HLECs treated with CM from the indicated ccRCC cells ($n = 4$) (ANOVA for statistics). (J) The protein expression of NAT10, ANKZF1, and VEGFC/D in the indicated ccRCC cells ($n = 3$). Results represented at least three independent experiments ($^*P < 0.05$, $^{**}P < 0.01$, $^{***}P < 0.001$). Abbreviations: ANKZF1, ankyrin repeat and zinc finger peptidyl tRNA hydrolase 1; NAT10, N-acetyltransferase 10; ccRCC, clear-cell renal cell carcinoma; RIP-seq, RNA immunoprecipitation-sequencing; DEGs, differentially expressed genes; ac^4C, N4-acetylcytidine; HLEC, human lymphatic endothelial cell; CM, conditioned medium; VEGFC/D, vascular endothelial growth factor-C/D; *CRYBG1*, crystallin beta-gamma domain containing 1; *CDIPT*, cdp-diacylglycerol-inositol 3-phosphatidyltransferase; *ATG16L2*, autophagy-related 16 like 2; GAPDH, glyceraldehyde-3-phosphate dehydrogenase.

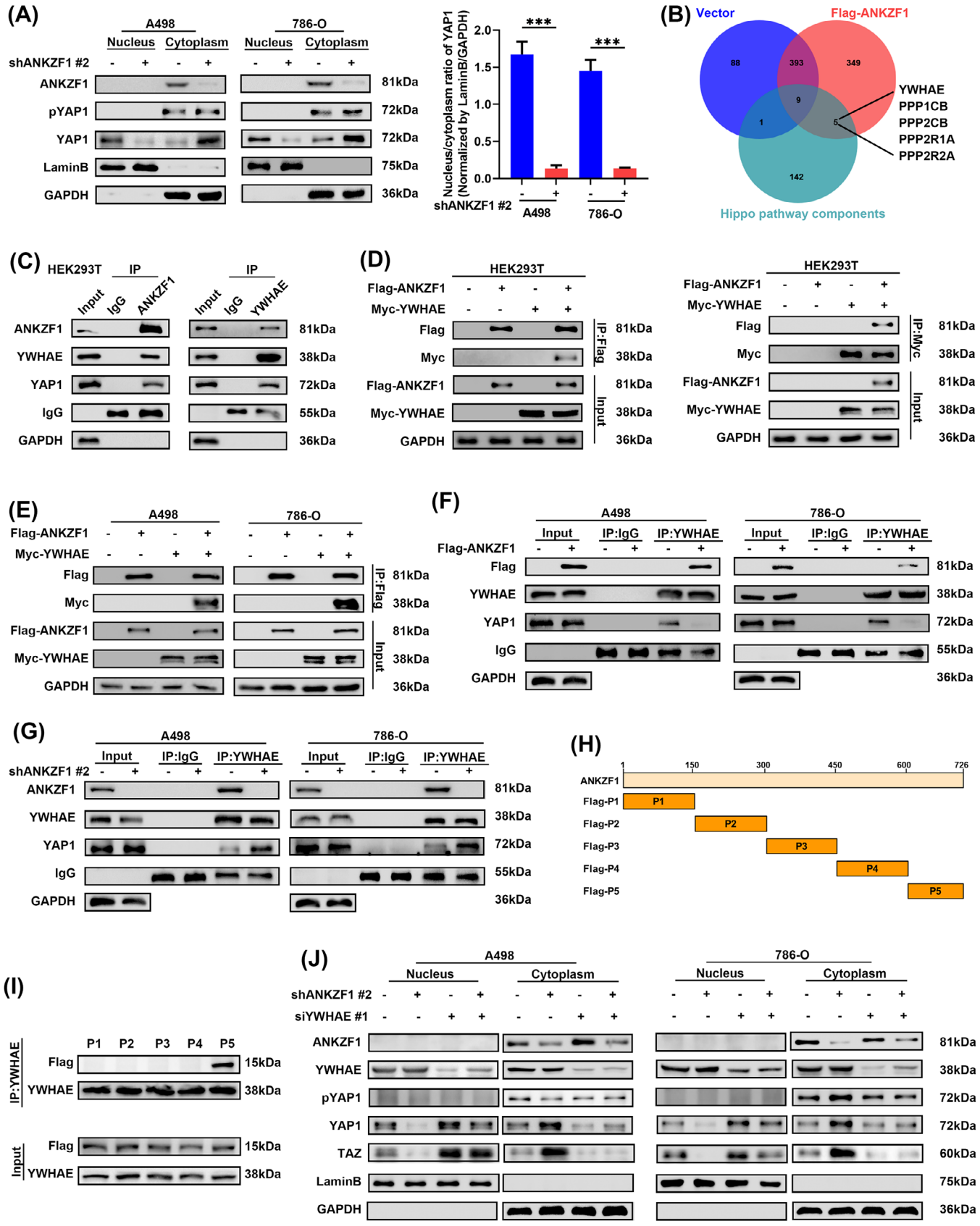

FIGURE 6 NAT10 inactivated the non-canonical Hippo signaling by enhancing the ANKZF1-YWHAE interaction. (A) Western blotting showed the subcellular localization of YAP1 after ANKZF1 knockdown ($n = 3$) (t-test for statistics). (B) Venn diagram of proteins pulled down through Flag-ANKZF1, proteins pulled down through Vector, and proteins in the Hippo pathway from the KEGG database. Peptides with an unused score > 1.3 (a credibility of more than 95%) were considered credible peptides, and proteins containing at least one unique peptide

common RNA chemical alterations and has a critical role in promoting the translational efficiency and stability of mRNA [23]. It was reported that both the distribution and the effect of ac^4C are different from those of N6-methyladenine [26]. A majority of ac^4C modifications occurred within the coding sequences and were related to substrate mRNA stability, while N6-methyladenosine residues showed a 3′-untranslated region localization bias and were associated with mRNA destabilization [26, 41]. Moreover, a previous study found that ac^4C modifications on the 5′ untranslated region and coding sequence had different impacts on mRNA translation and proposed that the role of ac^4C in mRNA translation was decided by the location where ac^4C modifications occurred [42]. Although the precise mechanisms through which NAT10-mediated ac^4C influenced mRNA translation and stabilization remain unclear, it did not prevent NAT10 from being a druggable target in cancers. Prior studies verified that NAT10-depleted tumor cells were more sensitive to doxorubicin therapy in hepatocellular carcinoma [43] and that breast cancer cells with chemical inhibition of NAT10 were hypersensitive to chemotherapy and radiotherapy [28]. In the present study, we found that NAT10-mediated ac^4C modification improved the stability of *ANKZF1* mRNA and caused the upregulation of ANKZF1 in ccRCC. These findings established a new explanation for how NAT10-mediated ac^4C modification functioned in ccRCC and provided a basis for the development of drugs targeting ac^4C modification in ccRCC.

Tumor lymphangiogenesis plays a pivotal role in regional lymph node metastasis [44]. It has been demonstrated that lymphangiogenesis was also significantly associated with the distant spread of cancer cells [8]. Consequently, an increasing number of researchers have shifted their research focus towards elucidating the regulatory mechanisms of tumor lymphangiogenesis [9]. MicroRNAs have been suggested to serve as robust post-transcriptional regulatory factors, exerting control over lymphangiogenesis [45]. It was proposed that miRNA-182-5p inhibited colon cancer tumorigenesis and lymphangiogenesis by directly targeting *VEGFC* [18]. In addition to microRNAs, RNA modifications also play a significant role in the post-transcriptional regulation of lymphangiogenesis [46]. For example, methyltransferase 3 (METTL3)-mediated N6-methyladenosine modifications stimulate lymphangiogenesis by regulating VEGFC expression [47]. In the study, we discovered that NAT10-mediated ac^4C modification promoted lymphangiogenesis in ccRCC by enhancing the mRNA stability of *ANKZF1*. Collectively, our findings not only emphasized the crucial role of post-transcriptional modifications in lymphangiogenesis but also established a significant association between ac^4C modification and tumor lymphangiogenesis.

Concurrently, in specific tumor contexts, VEGFC/D-VEGFR3-mediated lymphangiogenesis is also under the control of other signaling pathways. In pancreatic cancer, inhibition of the phosphatidylinositol-3-kinase/Akt pathway resulted in a subsequent downregulation of VEGFC expression, ultimately suppressing lymphangiogenesis and lymph node metastasis [48]. Zheng et al. [49] revealed that activation of the Wnt signaling heightened the secretion of VEGFC, thereby fostering the lymphatic metastasis of bladder cancer. Previous independent investigations have revealed that YAP1, the core effector of the Hippo pathway, regulated lymphangiogenesis by the VEGFC/D-VRGFR3 signaling pathway [50, 51]. Consistent with these findings, we discovered that NAT10-driven nuclear translocation of YAP1 led to an upregulation of VEGFC/D expression, consequently promoting lymphangiogenesis in ccRCC. Although VEGFC and VEGFD are pivotal lymphangiogenic factors in human cancers, the predominant emphasis has been on highlighting the lymphangiogenic role of VEGFC, with limited attention given to VEGFC-independent lymphangiogenic mechanisms [49, 52]. In this study, we observed that VEGFD might play a more critical role in NAT10-mediated lymphangiogenesis. While the NAT10-YAP1 axis concurrently upregulated the mRNA and protein levels of VEGFC/D, the increase in

were retained. The list of candidates in the Venn diagram has been deposited in the Science Data Bank (www.scidb.cn). (C) The endogenous ANKZF1-YWHAE interaction was determined by co-IP assays in HEK293T cells. (D) The exogenous ANKZF1-YWHAE interaction was determined by co-IP assays in HEK293T cells overexpressed Flag-ANKZF1 and/or Myc-YWHAE. (E) The exogenous ANKZF1-YWHAE interaction was determined by co-IP assays in ccRCC cells overexpressed Flag-ANKZF1 and/or Myc-YWHAE. (F) The YWHAE-YAP1 interaction was determined by co-IP assays in A498 and 786-O cells with Flag-ANKZF1 overexpression. (G) The YWHAE-YAP1 interaction was determined by co-IP assays in A498 and 786-O cells with ANKZF1 knockdown. (H) The diagrams show wild-type ANKZF1 (full length, 1-726) and its five truncations. (I) HEK293T cells were transfected with the truncated plasmids, followed by co-IP assays and Western blotting to examine the interaction between truncations of ANKZF1 and YWHAE. (J) Western blotting showed the subcellular localization of YAP1 in the indicated ccRCC cells. Results represented at least three independent experiments ($^*P < 0.05$, $^{**}P < 0.01$, $^{***}P < 0.001$). Abbreviations: ANKZF1, ankyrin repeat and zinc finger peptidyl tRNA hydrolase 1; NAT10, N-acetyltransferase 10; YWHAE, tyrosine 3-monooxygenase/tryptophan 5-monooxygenase activation protein epsilon; YAP1, yes1-associated transcriptional regulator; KEGG, kyoto encyclopedia of genes and genomes; co-IP, co-immunoprecipitation; pYAP1, phosphorylated YAP1; GAPDH, glyceraldehyde-3-phosphate dehydrogenase; PPP1/2CB, protein phosphatase 1/2 catalytic subunit beta; PPP2R1A/B, protein phosphatase 2 scaffold subunit Aalpha/Abeta.

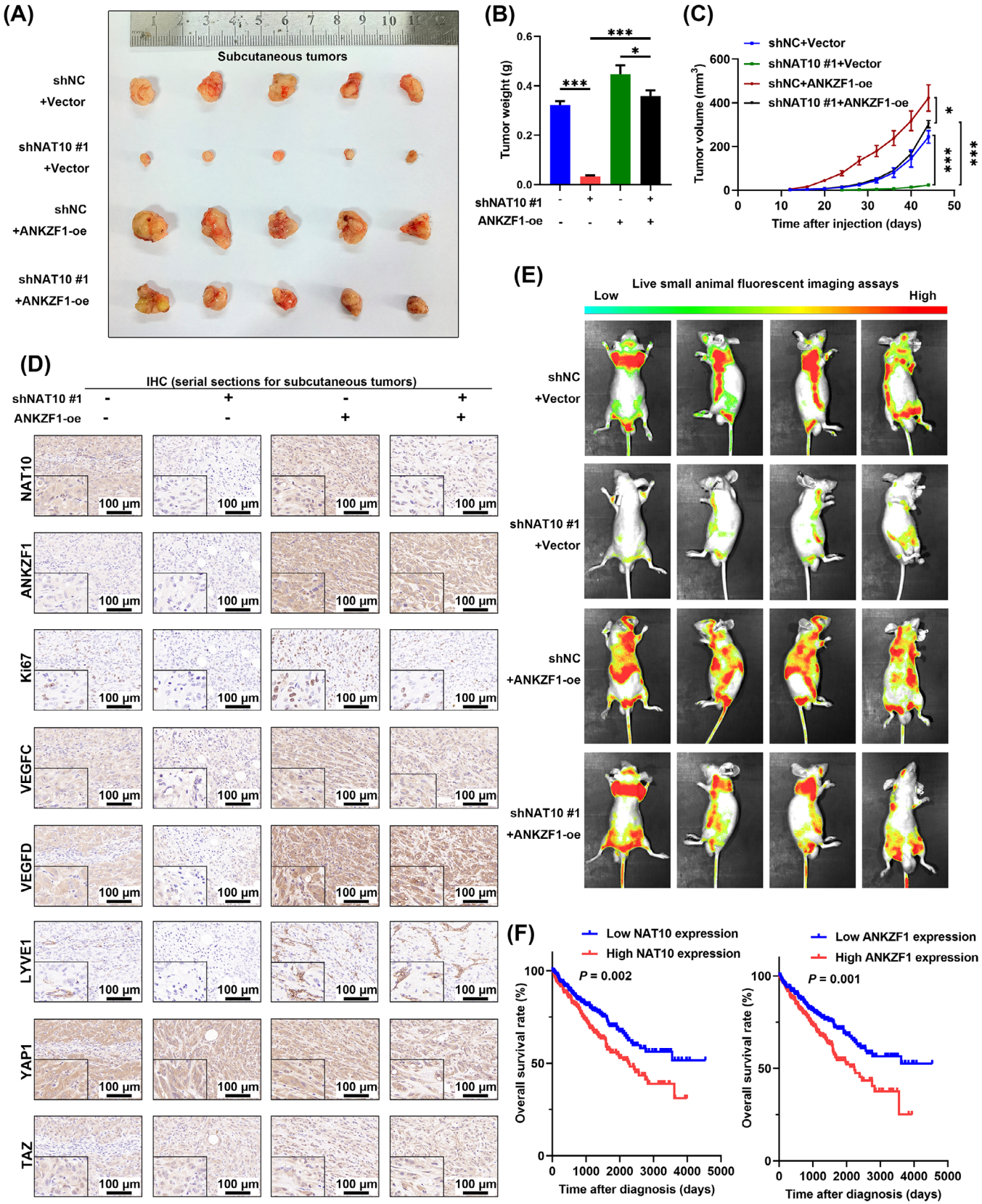

FIGURE 7 NAT10-ANKZF1 axis inactivated the non-canonical Hippo signaling and suppressed tumor progression in vivo. (A-B) Representative images of isolated subcutaneous tumors from nude mice in the indicated groups. Tumors were extracted and weighed after mice were euthanized ($n = 5$) (ANOVA for statistics). (C) Tumor size was measured every 4 days and the last measurement was performed on day 44 ($n = 5$) (ANOVA for statistics). (D) IHC staining for NAT10, ANKZF1, Ki67, VEGFC/D, YAP1/TAZ, and LYVE1 in the subcutaneous tumors ($n = 5$). The bottom left image is a 4 times magnified view of the original image's top-left corner. (E) Live small animal fluorescent

images of the indicated groups in the metastasis model. The images depict one mouse from each group in four distinct body positions. Nude mice were imaged eight weeks after performing tail vein injections of A498 cells ($n = 5$) (ANOVA for statistics). (F) The Kaplan-Meier analyses showed the association between the overall survival rates of ccRCC patients and the expression levels of NAT10 and ANKZF1. Patients were categorized into low and high subgroups using median expression (50%) as the cut-off (log-rank for statistics). Results represented at least three independent experiments (*$P < 0.05$, **$P < 0.01$, ***$P < 0.001$). Abbreviations: ANKZF1, ankyrin repeat and zinc finger peptidyl tRNA hydrolase 1; NAT10, N-acetyltransferase 10; IHC, immunohistochemistry; VEGFC/D, vascular endothelial growth factor-C/D; YAP1, yes1-associated transcriptional regulator; TAZ, tafazzin; LYVE1, lymphatic vessel endothelial hyaluronan receptor 1; Ki-67, marker of proliferation ki-67; TAZ, tafazzin.

VEGFD concentration induced by NAT10 overexpression in the CM was significantly more pronounced than that observed for VEGFC. This highlighted a possibility that the NAT10-regulated Hippo signaling might selectively participate in the maturation process of either VEGFC or VEGFD [51]. In summary, the present study elucidated a molecular mechanism of tumor lymphangiogenesis in ccRCC, providing new therapeutic targets for inhibiting the progression and lymphatic metastasis of renal cancer.

The present study had some limitations. Firstly, the underlying reasons for the upregulation of NAT10 in ccRCC remain unexplored. Secondly, despite our comprehensive utilization of bulk RNA-seq data, this data type inherently possesses limitations, such as the inability to capture cell-type specificity, providing only an averaged gene expression profile from a mix of cell types. Future investigations could employ cell-specific sequencing approaches, such as single-cell RNA sequencing, to further elucidate the role of NAT10 in ccRCC.

5 | CONCLUSIONS

In the present study, we found that aberrant upregulation of *ANKZF1* was caused by NAT10-mediated ac^{4}C modification in ccRCC. As a functional target of NAT10, ANKZF1 interacted with YWHAE, resulting in increased nuclear localization of YAP1. The NAT10/ANKZF1 axis-mediated

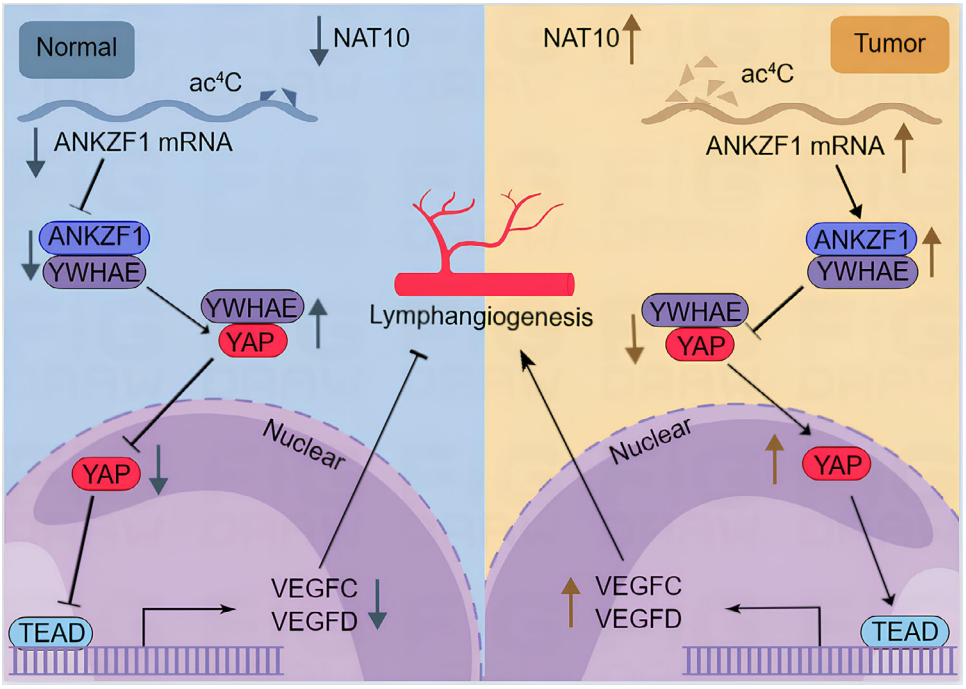

FIGURE 8 The mechanism scheme of NAT10 in ccRCC. NAT10-mediated ac^{4}C raised the expression of ANKZF1 in ccRCC; ANKZF1 interacted with YWHAE to promote the nuclear localization of YAP1, thereby activating the transcription of VEGFC/D. Then the NAT10/ANKZF1 axis-regulated non-canonical Hippo pathway promoted tumor progression and lymphangiogenesis in ccRCC. The mechanism scheme was drawn by using Figdraw (www.figdraw.com). Abbreviations: ANKZF1, ankyrin repeat and zinc finger peptidyl tRNA hydrolase 1; NAT10, N-acetyltransferase 10; VEGFC/D, vascular endothelial growth factor-C/D; YAP1, yes1-associated transcriptional regulator; YWHAE, tyrosine 3-monooxygenase/tryptophan 5-monooxygenase activation protein epsilon; ac4C, N4-acetylcytidine; TEAD, tea domain transcription factor.

nuclear import of YAP1 promoted the progression and lymphangiogenesis of ccRCC through the transcriptional activation of *VEGFC/D*. Together, these findings highlight a fundamental regulatory mechanism underlying non-canonical Hippo signaling and tumor lymphangiogenesis of ccRCC and suggest that inhibition of NAT10/ANKZF1 may yield clinical benefits for ccRCC patients.

DECLARATIONS

AUTHOR CONTRIBUTIONS

XZ and ZX designed the present study. DM, JS, and QL conducted the experiments. DM, DT, and CZ analyzed the data. DM wrote the manuscript. All authors read and approved the final manuscript.

ACKNOWLEDGEMENTS

This study was supported by the National Natural Science Foundation of China (81874090, 81972630, 82202911, 82300786).

CONFLICT OF INTERESTS STATEMENT

The authors declare no potential conflicts of interest.

DATA AVAILABILITY STATEMENT

Data generated in the present study are available from the corresponding author upon request. The sequencing and proteomic datasets have been deposited in Science Data Bank (https://www.scidb.cn/, Doi:10.57760/sciencedb.15742).

ETHICS APPROVAL AND CONSENT TO PARTICIPATE

Tissue samples were obtained from ccRCC patients with written informed consent. The present study was authorized by the ethics committee of Wuhan Union Hospital (IEC-072).

CONSENT FOR PUBLICATION

Not applicable.

ORCID

Xiaoping Zhang https://orcid.org/0000-0003-0218-3288

REFERENCES

1. Sung H, Ferlay J, Siegel RL, Laversanne M, Soerjomataram I, Jemal A, et al. Global Cancer Statistics 2020: GLOBOCAN Estimates of Incidence and Mortality Worldwide for 36 Cancers in 185 Countries. CA Cancer J Clin. 2021;71(3):209–49.
2. Jonasch E, Walker CL, Rathmell WK. Clear cell renal cell carcinoma ontogeny and mechanisms of lethality. Nat Rev Nephrol. 2021;17(4):245–61.
3. Siegel RL, Miller KD, Fuchs HE, Jemal A. Cancer statistics, 2022. CA Cancer J Clin. 2022;72(1):7–33.
4. Ljungberg B, Bensalah K, Canfield S, Dabestani S, Hofmann F, Hora M, et al. EAU guidelines on renal cell carcinoma: 2014 update. Eur Urol. 2015;67(5):913–24.
5. Jonasch E, Gao J, Rathmell WK. Renal cell carcinoma. BMJ. 2014;349:g4797.
6. Brown JE, Symeonides SN. Treatment Strategies in Metastatic Renal Cancer: Dose Titration in Clear Cell Renal Cell Carcinoma. Eur Urol. 2022;82(3):293–4.
7. Dudani S, de Velasco G, Wells JC, Gan CL, Donskov F, Porta C, et al. Evaluation of Clear Cell, Papillary, and Chromophobe Renal Cell Carcinoma Metastasis Sites and Association With Survival. JAMA Netw Open. 2021;4(1):e2021869.
8. Stacker SA, Williams SP, Karnezis T, Shayan R, Fox SB, Achen MG. Lymphangiogenesis and lymphatic vessel remodelling in cancer. Nat Rev Cancer. 2014;14(3):159–72.
9. Sundar SS, Ganesan TS. Role of lymphangiogenesis in cancer. J Clin Oncol. 2007;25(27):4298–307.
10. Hanahan D, Weinberg RA. Hallmarks of cancer: the next generation. Cell. 2011;144(5):646–74.
11. Leu AJ, Berk DA, Lymboussaki A, Alitalo K, Jain RK. Absence of functional lymphatics within a murine sarcoma: a molecular and functional evaluation. Cancer Res. 2000;60(16):4324–7.
12. Dieterich LC, Detmar M. Tumor lymphangiogenesis and new drug development. Adv Drug Deliv Rev. 2016;99(Pt B):148–60.
13. Stacker SA, Achen MG, Jussila L, Baldwin ME, Alitalo K. Lymphangiogenesis and cancer metastasis. Nat Rev Cancer. 2002;2(8):573–83.
14. Dieterich LC, Tacconi C, Ducoli L, Detmar M. Lymphatic vessels in cancer. Physiol Rev. 2022;102(4):1837–79.
15. Zhang Z, Helman JI, Li LJ. Lymphangiogenesis, lymphatic endothelial cells and lymphatic metastasis in head and neck cancer–a review of mechanisms. Int J Oral Sci. 2010;2(1):5–14.
16. Da MX, Wu Z, Tian HW. Tumor lymphangiogenesis and lymphangiogenic growth factors. Arch Med Res. 2008;39(4):365–72.
17. Achen MG, McColl BK, Stacker SA. Focus on lymphangiogenesis in tumor metastasis. Cancer Cell. 2005;7(2):121–7.
18. Yan S, Wang H, Chen X, Liang C, Shang W, Wang L, et al. MiR-182-5p inhibits colon cancer tumorigenesis, angiogenesis, and lymphangiogenesis by directly downregulating VEGF-C. Cancer Lett. 2020;488:18–26.
19. Ozardili I, Guldur ME, Ciftci H, Bitiren M, Altunkol A. Correlation between lymphangiogenesis and clinicopathological parameters in renal cell carcinoma. Singapore Med J. 2012;53(5):332–5.
20. Debinski P, Dembowski J, Kowal P, Szydelko T, Kolodziej A, Malkiewicz B, et al. The clinical significance of lymphangiogenesis in renal cell carcinoma. Med Sci Monit. 2013;19:606–11.
21. Horiguchi A, Ito K, Sumitomo M, Kimura F, Asano T, Hayakawa M. Intratumoral lymphatics and lymphatic invasion are associated with tumor aggressiveness and poor prognosis in renal cell carcinoma. Urology. 2008;71(5):928–32.
22. Lv J, Liu H, Wang Q, Tang Z, Hou L, Zhang B. Molecular cloning of a novel human gene encoding histone acetyltransferase-like protein involved in transcriptional activation of hTERT. Biochem Biophys Res Commun. 2003;311(2):506–13.

23. Dominissini D, Rechavi G. N(4)-acetylation of Cytidine in mRNA by NAT10 Regulates Stability and Translation. Cell. 2018;175(7):1725–7.
24. Kowalski S, Yamane T, Fresco JR. Nucleotide sequence of the "denaturable" leucine transfer RNA from yeast. Science. 1971;172(3981):385–7.
25. Oashi Z, Murao K, Yahagi T, Von Minden DL, McCloskey JA, Nishimura S. Characterization of C + located in the first position of the anticodon of Escherichia coli tRNA Met as N 4 -acetylcytidine. Biochim Biophys Acta. 1972;262(2): 209–13.
26. Arango D, Sturgill D, Alhusaini N, Dillman AA, Sweet TJ, Hanson G, et al. Acetylation of Cytidine in mRNA Promotes Translation Efficiency. Cell. 2018;175(7):1872–86 e24.
27. Hao H, Liu W, Miao Y, Ma L, Yu B, Liu L, et al. N4-acetylcytidine regulates the replication and pathogenicity of enterovirus 71. Nucleic Acids Res. 2022;50(16):9339–54.
28. Liu HY, Liu YY, Yang F, Zhang L, Zhang FL, Hu X, et al. Acetylation of MORC2 by NAT10 regulates cell-cycle checkpoint control and resistance to DNA-damaging chemotherapy and radiotherapy in breast cancer. Nucleic Acids Res. 2020;48(7): 3638–56.
29. Zheng X, Wang Q, Zhou Y, Zhang D, Geng Y, Hu W, et al. N-acetyltransferase 10 promotes colon cancer progression by inhibiting ferroptosis through N4-acetylation and stabilization of ferroptosis suppressor protein 1 (FSP1) mRNA. Cancer Commun (Lond). 2022;42(12):1347–66.
30. Li Q, Liu X, Jin K, Lu M, Zhang C, Du X, et al. NAT10 is upregulated in hepatocellular carcinoma and enhances mutant p53 activity. BMC Cancer. 2017;17(1):605.
31. Yang C, Wu T, Zhang J, Liu J, Zhao K, Sun W, et al. Prognostic and Immunological Role of mRNA ac4C Regulator NAT10 in Pan-Cancer: New Territory for Cancer Research? Front Oncol. 2021;11:630417.
32. Holmqvist A, Gao J, Adell G, Carstensen J, Sun XF. The location of lymphangiogenesis is an independent prognostic factor in rectal cancers with or without preoperative radiotherapy. Ann Oncol. 2010;21(3):512–7.
33. Yoshimatsu Y, Miyazaki H, Watabe T. Roles of signaling and transcriptional networks in pathological lymphangiogenesis. Adv Drug Deliv Rev. 2016;99(Pt B):161–71.
34. Wang Y, Xu X, Maglic D, Dill MT, Mojumdar K, Ng PK, et al. Comprehensive Molecular Characterization of the Hippo Signaling Pathway in Cancer. Cell Rep. 2018;25(5): 1304–17 e5.
35. Meng Z, Moroishi T, Guan KL. Mechanisms of Hippo pathway regulation. Genes Dev. 2016;30(1):1–17.
36. Basu S, Totty NF, Irwin MS, Sudol M, Downward J. Akt phosphorylates the Yes-associated protein, YAP, to induce interaction with 14-3-3 and attenuation of p73-mediated apoptosis. Mol Cell. 2003;11(1):11–23.
37. Yu XM, Li SJ, Yao ZT, Xu JJ, Zheng CC, Liu ZC, et al. N4-acetylcytidine modification of lncRNA CTC-490G23.2 promotes cancer metastasis through interacting with PTBP1 to increase CD44 alternative splicing. Oncogene. 2023;42(14): 1101–16.
38. Wiener D, Schwartz S. The epitranscriptome beyond m(6)A. Nat Rev Genet. 2021;22(2):119–31.
39. Boriack-Sjodin PA, Ribich S, Copeland RA. RNA-modifying proteins as anticancer drug targets. Nat Rev Drug Discov. 2018;17(6):435–53.
40. Zhang H, Zhai X, Liu Y, Xia Z, Xia T, Du G, et al. NOP2-mediated m5C Modification of c-Myc in an EIF3A-Dependent Manner to Reprogram Glucose Metabolism and Promote Hepatocellular Carcinoma Progression. Research (Wash D C). 2023;6: 0184.
41. Roundtree IA, Evans ME, Pan T, He C. Dynamic RNA Modifications in Gene Expression Regulation. Cell. 2017;169(7): 1187–200.
42. Arango D, Sturgill D, Yang R, Kanai T, Bauer P, Roy J, et al. Direct epitranscriptomic regulation of mammalian translation initiation through N4-acetylcytidine. Mol Cell. 2022;82(15):2797–814 e11.
43. Zhang X, Chen J, Jiang S, He S, Bai Y, Zhu L, et al. N-Acetyltransferase 10 Enhances Doxorubicin Resistance in Human Hepatocellular Carcinoma Cell Lines by Promoting the Epithelial-to-Mesenchymal Transition. Oxid Med Cell Longev. 2019;2019:7561879.
44. Zhang Q, Liu S, Wang H, Xiao K, Lu J, Chen S, et al. ETV4 Mediated Tumor-Associated Neutrophil Infiltration Facilitates Lymphangiogenesis and Lymphatic Metastasis of Bladder Cancer. Adv Sci (Weinh). 2023;10(11): e2205613.
45. Arcucci V, Stacker SA, Achen MG. Control of Gene Expression by Exosome-Derived Non-Coding RNAs in Cancer Angiogenesis and Lymphangiogenesis. Biomolecules. 2021;11(2): 249.
46. Sun R, Yuan L, Jiang Y, Wan Y, Ma X, Yang J, et al. ALKBH5 activates FAK signaling through m6A demethylation in ITGB1 mRNA and enhances tumor-associated lymphangiogenesis and lymph node metastasis in ovarian cancer. Theranostics. 2023;13(2):833–48.
47. Zhou J, Wei T, He Z. ADSCs enhance VEGFR3-mediated lymphangiogenesis via METTL3-mediated VEGF-C m(6)A modification to improve wound healing of diabetic foot ulcers. Mol Med. 2021;27(1):146.
48. Kong Y, Li Y, Luo Y, Zhu J, Zheng H, Gao B, et al. circNFIB1 inhibits lymphangiogenesis and lymphatic metastasis via the miR-486-5p/PIK3R1/VEGF-C axis in pancreatic cancer. Mol Cancer. 2020;19(1):82.
49. Zheng H, Chen C, Luo Y, Yu M, He W, An M, et al. Tumor-derived exosomal BCYRN1 activates WNT5A/VEGF-C/VEGFR3 feedforward loop to drive lymphatic metastasis of bladder cancer. Clin Transl Med. 2021;11(7):e497.
50. Hong SP, Yang MJ, Cho H, Park I, Bae H, Choe K, et al. Distinct fibroblast subsets regulate lacteal integrity through YAP/TAZ-induced VEGF-C in intestinal villi. Nat Commun. 2020;11(1):4102.
51. Song J, Dang X, Shen X, Liu Y, Gu J, Peng X, et al. The YAP-TEAD4 complex promotes tumor lymphangiogenesis by transcriptionally upregulating CCBE1 in colorectal cancer. J Biol Chem. 2023;299(4):103012.
52. Zhu J, Luo Y, Zhao Y, Kong Y, Zheng H, Li Y, et al. circEHBP1 promotes lymphangiogenesis and lymphatic metastasis of bladder cancer via miR-130a-3p/TGFbetaR1/VEGF-D signaling. Mol Ther. 2021;29(5):1838–52.

SUPPORTING INFORMATION

Additional supporting information can be found online in the Supporting Information section at the end of this article.

How to cite this article: Miao D, Shi J, Lv Q, Tan D, Zhao C, Xiong Z, et al. NAT10-mediated ac^4C-modified ANKZF1 promotes tumor progression and lymphangiogenesis in clear-cell renal cell carcinoma by attenuating YWHAE-driven cytoplasmic retention of YAP1. Cancer Commun. 2024;44:361–383. https://doi.org/10.1002/cac2.12523